RSC Advances

ROYAL SOCIETY OF CHEMISTRY

www.rsc.org/advances

Thermally Cross-linked and Sulphur Cured Soft TPVs Based on S-EB-S and S-SBR Blend

Pranab Dey [a], Kinsuk Naskar [a], Biswaranjan Dash [b], Sujith Nair [b], G. Unnikrishnan [b], Golok B. Nando [a*]

[a] *Rubber Technology Centre, Indian Institute of Technology Kharagpur, Kharagpur – 721302, India.*

[b] *CEAT Limited, PO: Chandrapura, Taluk: Halol – 389350, Dist.: Panchmahal, Gujarat, India.*

* Corresponding author: Tel.: +91 3222 283194;

E-mail addresses: golokb@rtc.iitkgp.ernet.in

Abstract

Thermoplastic vulcanizate (TPV) is a specific group of elastomer alloy (EA) where the rubber phase is selectively cross-linked by dynamic vulcanization and dispersed in the presence of a molten thermoplastic phase under intensive mixing. The development of binary blends, utilizing melt blending technology of poly[styrene-b-(ethylene-co-butylene)-b-styrene] triblock copolymer (S-EB-S) and solution polymerized styrene butadiene rubber (S-SBR) were investigated, as were the characteristic differences of these blends compared to other soft TPVs. Design of experiment (DOE) has been adopted to execute the optimum processing conditions in terms of mixing temperature, rotor speed and time of mixing by utilizing the Taguchi's L_9 methodology and the measure of confidence has been accomplished using standard statistical technique of analysis of variance (ANOVA). A novel thermally cross-linked (TCL) TPV has emerged as a by-product of DOE. Thereafter, a meticulous analysis and characterization have been conducted to understand the newly developed TPV system. Further, both semi-efficient vulcanizate (SEV) and efficient vulcanizate (EV) sulphur based curing systems have been designed by adopting the optimized processing conditions to cure the rubber phase and a comparative study has been organized among TCL, SEV and EV systems. Dynamic mechanical analysis (DMA) has revealed reduced rolling resistance for EV cured TPVs compared to SEV and TCL cured systems, while still maintaining good wet grip by comparing the loss tangent values. Theoretical calculation of viscoelastic properties by adopting Kerner model predicts primarily co-continuous morphology for the TPV systems, which is in well accordance with the experimental and morphological observations.

Keywords: Thermoplastic vulcanizates, design of experiment, thermal cross-linking, dynamic mechanical analysis, kerner model.

1. Introduction

Cross-linked rubber blends cannot be recycled because of their inherent lack of melt processability by shaping operation, as most of the thermoplastics. Conventional recycling process involves the generation of ground rubber (GR) or crumb rubber (CR) by suitable reclaiming and devulcanization processes,[1-3] which lead them to be considered as elastomeric alloys (EAs),[4-6] when added as soft fillers in a thermoplastic matrix. Ironically, the interphase incompatibility between the thermodynamically immiscible polymers reduces its effectiveness to be considered as thermoplastic elastomers (TPEs). TPEs are a class of material that combines the good elastic properties of physically cross-linked rubbers with the melt processability of thermoplastics[7-9]. TPEs can be classified as multiphase materials that consist of a rigid thermoplastic phase and a soft elastomer phase. At the service temperature, the hard blocks cluster together to form small domains, which act as physical cross-links between the soft blocks[10] (**Figure 1(a)).** Above the glass transition temperature (T_g) or melting temperature (T_m) of the hard blocks, the physical cross-links disappear and the material becomes melt processable. Thermoplastic vulcanizates (TPVs), on the other hand, is a specific group of TPEs where the rubber phase is cross-linked by dynamic vulcanization and dispersed in the presence of a molten thermoplastic phase[11] (**Figure 1(b)**). It exhibits elastomer-like properties: such as lower compression set, lower stiffness, greater resistance to fatigue, better resistance to heat and chemicals etc.[12, 13] whereas still retaining the melt processability like thermoplastics. These phenomenal qualities led themselves as a potential competitor to the fast growing rubber market[14] for the last two decades and gaining considerable momentum from various industries such as automotives, electronics, buildings etc.

The dynamic vulcanization process was first reported by Gessler and Haslett[15] in 1962 and then subsequently developed by Fisher[16], Coran and Patel[17, 18] and Coran et al[19]. The research was further continued and advanced by Abdou-Sabet and Fath[20] and Mousa et al[21]. Later on, a meticulous reviewed was conducted by Babu and Naskar on the recent development on different classes of TPVs[22].

S-EB-S is a hydrogenated styrenic triblock copolymer which is primarily used as a compatibilizer for the binary blend systems[23]. However, several researchers have reported the blend of S-EB-S with polypropylene (PP) to prepare TPEs[24-26]. Sengupta et al. reported the

comparative study of the oil extended S-EB-S/PP blend with PP/EPDM TPV[27]. Sengers et al. investigated the rheological properties of PP/S-EB-S blends[28, 29]. Subsequently, Ahmad et al. prepared highly transparent TPE from isotactic PP and S-EB-S triblock copolymer[30]. Picchioni et al. studied the mechanical and thermal behavior of polystyrene (PS)/S-EB-S blend[31]. Bayan has patented (1990) a thermoplastic elastomer composition produced by dynamic vulcanization of SBR and a co-continuous matrix of SEBS and PP for biomedical applications[32]. In addition, Lopez et al. developed and patented (2011) the tire tread which comprises a hydrogenated TPE (S-EB-S) and conventional di-ene elastomers e.g NR, SBR etc.[33] Therefore, to the best of our knowledge, there is no literature available which in-detail has investigated the various properties of TPVs constituted by S-EB-S and S-SBR blend as a potential competitor of PP/EPDM or PP/EOC TPVs (dynamically cured by peroxide) for automobile applications. The latter mentioned TPVs have already been widely studied and are commercially available because of their superior properties suitable for automotive applications. However, they fail to perform under dynamically loaded conditions essential for automotive ancillary applications such as tires. For dynamic products like tires, flexibility is an important criterion which is achieved *via* sulphur vulcanization due to the formation of poly-sulphide and di-sulphide linkages. Hence, sulphur vulcanization is preferred over peroxide curing where flexibility is restrained because of the carbon-carbon link formation (higher bond strength). Moreover, high hardness of the mentioned TPVs is a major concern that severely affects the resilience and flexibility of the final product[34]. It is found that PP/EPDM or PP/EOC TPVs containing 40 weight percentage of PP depict hardness to the extent of 90 Shore A[35]. Several attempts have been made to reduce the hardness through oil extension as well as by reducing the thermoplastic component but those techniques rather lead to distinct reduction in mechanical properties[36]. Nevertheless sulphur cured PP/EPDM TPVs depict excellent mechanical properties but a severe stench problem during production and processing, high melting point of PP and poor thermal and UV stability of the sulphur cross-links restrict its commercial viability[37]. Moreover, the PP phase in the peroxide cured TPVs tend to undergo degradation *via* β-scission of the polymer backbone under the action of the free radicals generated by the decomposition of the peroxide. To overcome these problems, a new TPV system has been introduced based on S-SBR and S-EB-S blends in which sulphur vulcanization system has been adopted to cure the rubber phase and the TPV has registered good mechanical property with reduced hardness suitable for static as well as dynamic

applications. The close proximity of solubility parameters of both S-EB-S and S-SBR leads to the initial assumption that dynamic vulcanization would result in such a TPV which can fulfill the growing demands of automotive applications.

The primary objective of this investigation is to develop and optimize the melt mixing process of S-EB-S and S-SBR binary blends through DOE by utilizing Taguchi's L_9 methodology followed by ANOVA to identify the most influential process parameters for the blend processing. **Table 1** provides three parameters A, B, and C each of which contains three levels with nine different combinations which all together constitute L_9 orthogonal array, with nine rows indicating the prototypes of experiments. Thereafter, a semi-efficient vulcanizing system (SEV) and efficient vulcanizing system (EV) have been designed by partially adopting the optimized processing conditions to cure the rubber phase and a comparative study has been conducted to understand the characteristic differences between the respective TPVs.

2. Experimental

2.1. Materials

S-EB-S (trade name Kraton® G1657) is a clear, linear triblock copolymer based on styrene and ethylene/butylene having polystyrene content of 13%. Density of S-EB-S is 0.90 gm/cc and the melt flow index is 22 gms/10 min. at 230°C/5 kg. The supply comes from Kraton Polymer of Belgium in the physical form of dusted pellet. Another polymer i.e. S-SBR is procured from Dycon Chemicals, Mumbai, India having a polystyrene content of 23.5%. The chemical structures of S-EB-S and S-SBR are given in **Figure 2(a) and (b).** The solvent toluene was obtained from Merck Specialities Private Ltd, India. Accelerator activators i.e. Zinc oxide (Zinc content 82%) and stearic acid (max. ash content 0.1%) were procured from Sunrise Overseas, India. Accelerators CBS (N-cyclohexyl-2-benzothiazolesulfenamide) and TMTD (tetramethyl thiuram disulfide) obtained from Lanxess Rubber Chemicals, India, having melting point 98°C and 142°C as well as ash content below 3% respectively. Finally, the cross-linking agent sulphur powder (max. ash content 0.2%) was procured from Triveni Chemicals, India.

2.2. Preparation of blends

Melt blending of S-EB-S TPE and S-SBR rubber have been done in a Brabender Plastograph EC (Digital 3.8-kW motor, a torque measuring range of 200 Nm and a speed range from 0.2 to 150 min^{-1}). Three different stages were adopted to prepare the blends. In the first stage, the S-EB-S and S-SBR were melt blended at different weight percentage levels (from 0% to 100%) and subsequently their mechanical properties were measured to ensure the effect of blend ratios over the mechanical properties of the system. The final selection of blend ratio was done based on the experimental output to perform the design of experiment (DOE) for optimizing the processing parameters. The experimental observations are depicted in later section.

In the second stage, DOE was performed by adopting Taguchi's L_9 methodology, as exemplified in **Table 2.** S-EB-S was first loaded into the chamber and allowed to be melted in the mixer for 1 min, and then S-SBR was added and melt-blended according to the specified conditions. A detailed statistical analysis was performed to optimize the processing conditions for maximizing the product performance with the resultant blended specimens.

In the third stage, binary blended TPVs with a composition of 50/50 wt% S-EB-S/S-SBR were prepared **(Table 3)** by partially adopting the optimized processing conditions. A semi-efficient (SEV) and efficient (EV) sulphur based curing systems were used to cross-link the elastomer phase. While mixing, S-EB-S was first loaded into the chamber and allowed to melt 1 min, and then S-SBR was added and melt-blended according to the specified conditions which took about 1 min. Thereafter, zinc oxide and stearic acid were added. Finally the sequence ended up with the addition of sulphur and accelerator. Mixing was continued until the plateau mixing torque was reached and the resulting TPVs were then quickly removed and passed through a two-roll mill having a close nip-gap at room temperature and then sheeted out for subsequent operations. The torque-time curves obtained during the melt blending process of TPV formation are given in **Figure 3.** The delta-torque value obtained was appeared to be higher for EV cured system and numerically the delta-torque difference is about 4.2 Nm for the mentioned TPVs.

2.3. Preparation of moulded specimens

The sheet obtained from the two-roll mill was compression moulded in a hydraulic press (Moore Presses, George E. Moore & Sons Birmingham Ltd, UK) at 160°C for 4 min, under a pressure of 5 MPa, to form tensile sheets of about 2 mm thick. The mould was allowed to cool under

pressure to the ambient temperature before ejecting the sheets from the mould cavity. Dumb-bell specimens were punched out of the sheets using standard cutting die.

2.4. Mechanical Properties

The mechanical properties of the blends were determined as per ASTM D 412 (A dumbbell specimen was placed in the grips of the testing machine, using care to adjust the specimen symmetrically to distribute tension uniformly over the cross section) using a Hounsfield H25KS universal testing machine at a crosshead speed of 500 mm/min. The hardness of the samples was determined using a Shore A Durometer hardness tester as per ASTM D 2240 (specimens having min. 6 mm. of thickness were subjected to the direct indentation through parallel contact of the specimen to the durometer pressure foot without shock and with just sufficient force to overcome the spring force). Testing of all the samples were carried out at 25°C.

2.5. Characterization

2.5.1. FT-IR spectroscopy

Thin films (0.5 mm) of the blends prepared during DOE were characterized using Perkin-Elmer, version 5.0.1 spectrometer. A random sampling was done from the blended mass to cast the thin films prepared by compression moulding operation in hydraulic press. FT-IR spectra was then recorded at room temperature and collected over the range of 4400–400 cm^{-1}.

2.5.2. Overall cross-link density by equilibrium solvent swelling method

Swelling experiments were conducted on small rectangular (approximately 20 × 10 × 2 mm) specimens in toluene at room temperature for 72 hours. At the end of immersion period the sample was removed, gently wiped with tissue and transferred to the weighing balance to obtain the swollen weight of the sample. From the degree of swelling an overall cross-link density was calculated by using Flory-Rehner equation[38-40] (Equation 1) relative to the (S-SBR and S-EB-S) phases as expressed by (v + S-EB-S). The latter was done in order to correct for a part of the S-EB-S, being extracted as amorphous phase[41, 42].

$$(v + S\text{-}EB\text{-}S) = -\frac{1}{V_s} \times \frac{\ln(1-V_r)+V_r+\chi(V_r)^2}{(V_r)^{2/3}-0.5\times V_r} \qquad (1)$$

where,

ν = number of moles of effectively elastic chains per unit volume of S-SBR [mol/ml] (cross-link density).

V_s = molar volume of solvent (toluene).

χ = polymer-swelling agent interaction parameter, taken as 0.38 for both S-SBR and toluene at 25°C[43, 44].

V_r =Volume fraction of rubber in the swollen network and V_r can be expressed as

$$V_r = \frac{1}{A_r + 1} \qquad (2)$$

where,

A_r = Ratio of the volume of absorbed toluene to that of S-SBR after swelling.

2.5.3. Scanning electron microscopy:

ZEISS EVO 60 **(**Carl ZEISS SMT, Germany**)** scanning electron microscopy (SEM) was used to study the surface topography of the cryogenic fractured specimens after complete etching of the TPE phase (S-EB-S) using toluene solvent at 25°C for 72 hrs. After evaporating the solvent at 60°C for 24 hrs, the gold coated etched specimens were then subjected to SEM micrography.

2.5.4. Atomic force microscopy:

Intermittent contact mode atomic force microscopy, ACAFM (Agilent 5500 Scanning Probe Microscope) was used to investigate the morphology of the TPVs thin films prepared by compression moulding at 5 MPa pressure at 160°C for 4 min to support the SEM observations. The resonance frequency of the tip was 146-236 kHz and the force constant was 48 N/m.

2.5.5. Melt rheological study

The rheological measurements of TPVs were carried out by a Rubber Process Analyzer (RPA 2000, Alpha Technology, USA). Frequency range was selected between 0.5 Hz to 32 Hz and a strain controlled dynamic frequency sweep test was applied. Similarly, for frequency controlled dynamic strain sweep, the strain range was selected in between 0.7% to 1250%. The

measurements were done in ambient atmosphere at a temperature of 120°C. During each experiment, the temperature was maintained at the desired constant value by constantly heating the sample.

2.5.6. Dynamic Mechanical Analysis:

DMA measurements were performed with a Dynamic Mechanical Analyzer, Metravib 50 N, France. The temperature sweep experiments were carried out using tension mode of the DMA instrument over a temperature range of –100°C to +100°C, at a rate of 2°C /min. The samples were scanned at a frequency of 10 Hz, and a strain level of 10 μm which was well within the linear viscoelastic (LVR) region. The storage modulus (E′), loss modulus (E″), and the loss tangent (tanδ) were recorded as a function of temperature.

2.6. Design of experiments and S/N ratio

DOE is a powerful analytical tool for modeling and analyzing the influence of control factors on performance output. A plenty of designs (response surface, mixture design, factorial design etc.) available today to measure the control parameters, but in between that Taguchi method is a well known experimentally established technique used in the design of experiments for achieving optimum conditions to improve quality performance based on a mathematical approach[45]. This method utilizes a minimum number of experiments to analyze the effect of multiple factors by determining the most significant parameters contributing to the final deliverables. The implementation strategy of Taguchi method for optimizing the processing parameters is presented[45] in Scheme 1 These experiments are conducted in accordance to fulfill the following objectives: (1) to find out the best or optimal conditions for the product or process, (2) to identify the contribution of individual factors, and (3) to estimate the response under optimal conditions[46].

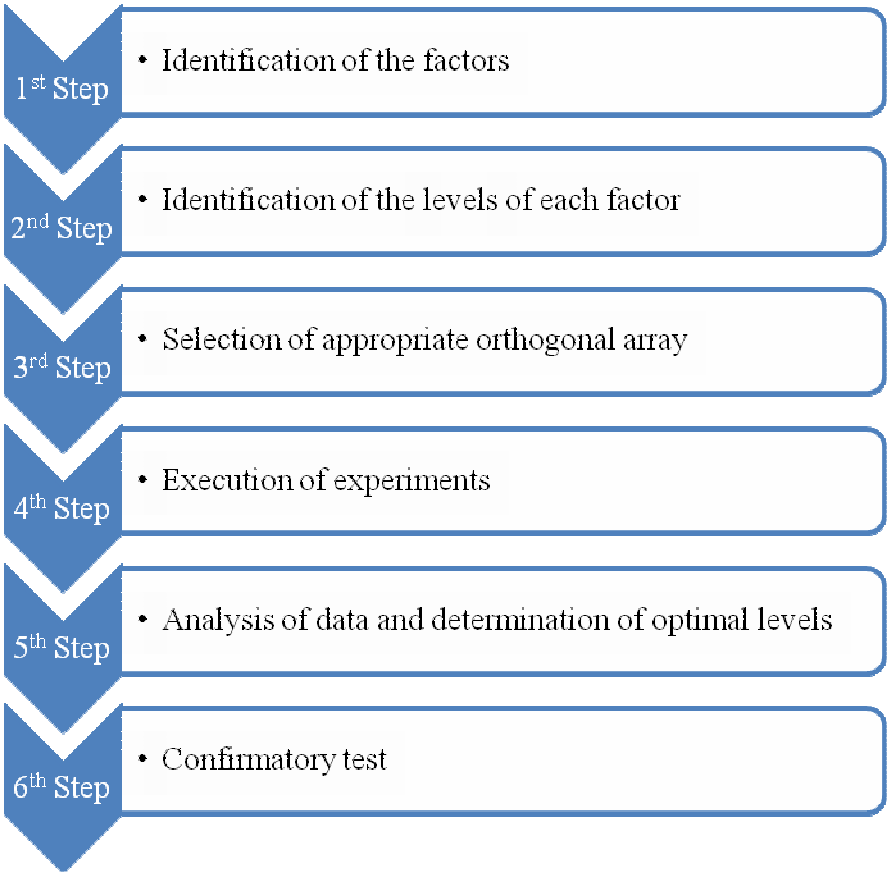

Scheme 1. Step by step schematic representation of Taguchi method.

The experiments have been designed by varying the process parameters, such as temperature, rotor speed and mixing time, using the L_9 orthogonal array and S/N ratio of DOE for the blend of S-EB-S/S-SBR (50:50). The orthogonal array testing strategy has been adopted to analyze the experimental data. The factors that control the blend characteristics and their levels are presented in Table 1. The three levels for each factor are designated as 1, 2 and 3. The blends have been designated as e.g. SS 3, indicating the 50:50 blend ratios of S-EB-S/S-SBR, and the number of experiments has been indicated as SS 1 to SS 9 for all the nine experiments. Two major tools are used in this robust design[47, 48]:

- Signal to noise ratio, which assesses the quality by emphasizing the variations.
- Orthogonal arrays, which accommodate several, design factors simultaneously.

In a conventional full factorial experiment it would require $3^3 = 27$ runs to study three factors at three levels, whereas Taguchi's factorial experiment approach reduces it to only 9 runs, offering

a great advantage in terms of experimental time and cost. The S/N ratio may be divided into three categories, as given below[49]:

(i) Nominal (the best characteristic), which can be calculated from equation (3)

$$S/N = -10\ log\frac{1}{n}[\sum_{i=1}^{n}(y_i - M)^2] \quad (3)$$

(ii) Smaller (the better characteristics), which can be calculated using equation (4)

$$S/N = -10\ log\frac{1}{n}(\sum_{i=1}^{n} y_i^2) \quad (4)$$

(iii) Larger (the better characteristics), which can be calculated using equation (5)

$$S/N = -10\ log\frac{1}{n}\left(\sum_{i=1}^{n}\frac{1}{y_i^2}\right) \quad (5)$$

Where, M is the average of the observed data, n is the number of observations and y_i is the observed data. The higher is the S/N ratio, the better the results. In order to understand the impact of various control factors on the response of experimental data, it is desirable to develop the ANOVA to find the significant factors. The use of ANOVA gives a clear evidence of degree of variations and statistical quality control associated with the parameters and their levels. From the analysis, it becomes easier to identify the effectiveness of the control factors on the ultimate blend properties. ANOVA has been established based on sum of the square (SS), the degree of freedom (DF), mean square (MS), F-ratio, P value and the percentage of contribution to the total variation. These parameters can be calculated[50] as follows:

The total sum of squares SS_T can be calculated as:

$$SS_T = \sum_{i}^{m} n_i^2 - \frac{1}{m}[\sum_{i=1}^{m} n_i]^2 \quad (6)$$

Where, m and n_i represent the number of experiments and the S/N ratio at the i^{th} test respectively.

Likewise, sum of squares for the tested factors (SS_p) can be represented as follow:

$$SS_p = \sum_{j=1}^{t} \frac{(S_{nj})^2}{t} - \frac{1}{m}\left(\sum_{i=1}^{m} n_i\right) \quad (7)$$

Where, p denotes one of the tested factors. j, t and S_{nj} represents the level number, the repetition of each level of the factor p and the sum of the S/N ratio involving this factor and level j respectively.

Degrees of freedom (DF) from each source can be calculated by using the formula (n - 1). Where, n is the total number of levels in a factor or total number of observations.

Mean squares (MS) can be found by dividing the sum of squares (SS_p) by the degrees of freedom (DF).

F-ratio can be calculated by dividing the factor MS by the error MS. This ratio is used to determine the significance of a factor.

Finally, the percentage contribution (P_C) from each factor can be calculated as follow:

$$P_C(\%) = \frac{SS_p}{SS_T} \times 100 \quad (8)$$

For each designed parameter, ANOVA provides the degree of freedom (DF), the sequential sums of squares (Seq SS), the adjusted (partial) sums of squares (Adj SS), the adjusted mean squares (Adj MS), the F statistic from the adjusted means squares, and percentage contribution (P_C). These parameters are then used for the quantitative validation of Taguchi results through identifying the optimum processing conditions.

3. Results and Discussion

3.1. Analysis of DOE

3.1.1. Mechanical Properties obtained from DOE

Figure 4 describes the effect of blend ratios over the mechanical properties of the S-EB-S/S-SBR blends mixed at different weight percentage. The virgin S-EB-S exhibits a tensile strength of 17.1 MPa and elongation at break of 1322%. On addition of S-SBR into S-EB-S, the tensile strength and elongation at break start reduction and reach a minimum of 2.9 MPa and 942% respectively for 50:50 blends of S-EB-S/S-SBR. This decrease in tensile strength and elongation

at break of the S-EB-S/S-SBR blend has been explained, which is due to the gross immiscibility between the two blend components and also due to the lower modulus of S-SBR rubber. Based on this observation, it has been presumed that the effect of processing conditions can be well understood for the blend of 50:50 weight percentage where neither S-EB-S nor S-SBR will contribute as major component. Nine blends were then designed by varying the mixing parameters, i.e. temperature, time and rotor speed, at three levels each. These blends are designated from SS 1 to SS 9 and the experimental outcome is summarized in **Table 4**. It is interesting to observe that, as the mixing temperature rises, a decrease in tensile strength as well as elongation at break is observed for (50:50) S-EB-S and S-SBR blends. In all the cases of the blends (except SS 1 and SS 2) where the mixing parameters are kept relatively higher, a decrease in physical properties is observed. SS 9 is found to exhibit the lowest tensile strength of 2.8 MPa and elongation at break at 389% among all the blends studied. The torque-temperature curves obtained during the melt blending process are given in **Figure 5.** For all cases (unlike SS 1) the torque-time curves adopt a positive slope after a certain point of time while mixing. This may be due to the formation of partial thermal cross-links and the same has been discussed latter in-detail. For SS 1, the mixing parameters are not severe enough to cause the same and thus the curve levels off at the end of mixing. Thermal cross-linking, on the other hand, increases the surface tension of the rubber phase[51, 52] which eventually results in a phase separated system due to the increase in gross immiscibility between the blend components. Now changing the mixing parameters from SS 2 to SS 9, make the blends more prone towards thermal cross-linking which thereby leads to the higher phase separation for the blends processed at elevated processing conditions (SS 6, SS 8, SS 9 etc.). These phase separated blends cannot cause sufficient stress transfer during the tensile stretch and thus ends-up with poor mechanical properties.

3.1.2. Signal to noise ratio and ANOVA results

Taguchi's method uses a logarithmic function of the desired output as the statistical measure of performance called signal to noise ratio (S/N), to serve as objective function for optimization. Defined as the ratio of the mean (signal) to the standard deviation (noise), it considers both the mean and variability into account. There are three categories of S/N ratio: lower-the-better (LTB), higher-the-better (HTB), and nominal-the-best (NTB). The parameter level combination which maximizes the appropriate S/N ratio is the optimum setting. For instance, in the case of

maximizing the tensile strength and elongation at break, HTB (i.e. equation 5) characteristic needs to be used. Response table for signal to noise ratio for tensile strength (TS) is given in **Table 5** and the main effect plot for the same is given in **Figure 6(a).** Similarly, Response table for signal to noise ratio for elongation at break (EB) is given in **Table 6** and the main effect plot for the same is given in **Figure 6(b)**. Furthermore, the statistically significant parameters are determined by analysis of variance (ANOVA). ANOVA results for TS and EB are given in **Table 7** and **Table 8** respectively. With the S/N ratio and ANOVA analysis, the optimal combinations of the process parameters have been predicted.

3.1.3. Tensile Strength

From the response table (**Table 5**) and main effect plot (**Figure 6(a)**) it is clear that first processing condition (1-1-1) i.e. 160°C temperature, 60 rpm rotor speed and 10 min. of mixing is depicting the optimum processing condition and rotor speed is the main contributing factor here. On the other hand, ANOVA calculates the F-ratio (**Table 7**), which is the ratio between the regression mean square and the mean square error, as the measure of significance of the parameters under investigation with respect to the variance. In general, when F value increases, the significance of the parameter also increases. ANOVA table shows the percentage contribution of each parameter. It is seen that parameter rotor speed has got the maximum significant influence on the tensile strength at the confidence level of 91.39%. The corresponding high F-ratio and low P-value corroborate this result.

3.1.4. Elongation at break

From the response table (**Table 6**) and main effect plot (**Figure 6(b**)) it is clear that first processing condition (1-1-3) i.e. 160°C temperature, 60 rpm rotor speed and 6 min. of mixing has depicted the optimum processing condition and temperature is the main contributing factor here. Since 1-1-3 set does not exist in Taguchi L_9 table, therefore a separate set was prepared to verify the DOE predicted value with the experiment. Experimentally EB value appeared to be 1185% against the DOE predicted value of 1191% and TS value appeared as 4.2 MPa. On the other hand, ANOVA calculates (**Table 8**) temperature had got the maximum significant influence on the elongation at break at the confidence level of 97.52%. The corresponding high F-ratio and low P-value corroborate this result.

From the main effect plot and response table it is clear that first processing condition (1-1-1) i.e. 160°C temperature, 60 rpm rotor speed and 10 min. of mixing is depicting the optimum processing condition for optimum tensile strength and rotor speed is the main contributing factor here. On the other hand, the processing condition (1-1-3) i.e. 160°C temperature, 60 rpm rotor speed and 6 min. of mixing is depicting the optimum processing condition for optimum elongation at break and temperature is the main contributing factor here. Since from the application point of view both TS and EB are important, therefore we chose (1-1-1) i.e. 160°C temperature, 60 rpm rotor speed and 10 min of mixing time over the (1-1-3) i.e. 160°C temperature, 60 rpm rotor speed and 6 min of mixing time as the optimum processing condition for the S-EB-S/S-SBR (50:50) blend by compromising 3% loss in EB over the 0.2 MPa gain in TS in the first case of Taguchi composition.

3.1.5. Interaction of design parameters

Interactions Plot creates a single interaction plot for two factors, or a matrix of interaction plots for three to nine factors. An interaction plot is a plot of mean for each level of a factor with the level of a second factor held constant. These are useful for judging the presence of interactions[53]. In this study, there are three design parameters. As a result, the interaction plot is a matrix of plots shown in Figures **7(a) and (b)** for the tensile strength and elongation of break properties, respectively. Interaction is present when the response at a factor level depends upon the level(s) of other factors. Parallel lines in an interaction plot indicate no interaction. The greater the departure of the lines from the parallel state, the higher the degree of interaction. Figure **7(a) and (b)** represents a significant degree of interaction between the parameters because the interaction plots do not contain any parallel curves.

3.2. Thermal cross-link formation

As mentioned earlier that the mechanical properties are getting deteriorated at elevated processing conditions and the same is well evident from the mechanical property data shown in **Table 4.** Now, reconsideration of the torque-time curves (**Figure 5**) reveals an abnormal trend in case of SS 6, SS 8 and SS 9 mixing curves. There is a gradual increase in the mixing torque followed by maxima and then there is a gradual decrease followed by a little increment. It has been assumed that at higher temperature, rotor speed and time there is a definite formation of

thermal cross-link which leads to the increase in torque value. But, after thermal cross-link formation the cross-linked rubber droplets float into the TPE matrix and get slipped past each other at the rotor and the chamber wall. This leads to the reduction in mixing torque followed by a little increase, due to the increase in the thermal cross-links, as the mixing time prolonged. To verify the assumption, first all of the nine Taguchi blends (equal sized measured weight pieces) have been swelled in toluene solvent for one week. It has been found that all of the blends have shown complete solubility in toluene unlike the case for SS 6, SS 8 and SS 9 which did not dissolve but swelled. Thereafter, the cross-link density has been determined using equilibrium solvent swelling method by Flory-Rehner equation (**Figure 8**). It appears that the cross-link formation is highest for the blend of SS 9 followed by SS 6 and SS 8. Now, it is established that higher cross-link formation in one phase increases the interphase incompatibly leading to the gross immiscibility between the two blend components. That is why SS 9 is depicting poorest mechanical property compared to SS 6 and SS 8.

3.2.1. Infrared spectroscopic analysis

Infrared spectroscopic technique is extensively used to identify specific changes that occur in various polymer systems[54]. **Figure 9** shows the FTIR spectra of normal (SS 1) and thermally cross-linked (SS 9) Taguchi blends. The presence of peak corresponding to 1638 cm^{-1} ($C=C_{str}$) confirms the presence of unsaturated carbon-carbon double bond[55] in case of SS 1. On the other hand, SS 9 exhibits a very weak peak of very low intensity (almost vanish) at the same stretching frequency for unsaturated carbon-carbon double bond. This clearly confirms the formation of partial thermal cross-link in case of SS 9. The same phenomenon has been observed for the remaining compositions (SS 6 and SS 8) and the repetitive results confirm the presence of thermal cross-link in the compositions processed at higher processing conditions.

3.2.2. Morphology study

3.2.2.1. Atomic Force Microscopy

To understand the morphology of the thermally cross-linked TPVs, further investigation has been done by atomic force microscopy. **Figure 10(a)** reflects the phase morphology and **Figure 10(b)** represents the surface topography of the thermally cross-linked TPV (SS 9). The light yellow regions in the phase and topography images represent cross-linked rubber particles,

which are seemed to be dispersed in the TPE matrix. The particle size of the dispersed phase has been given in the respective histogram plot (**Figure 10(c))**. Now, if we recall the mixing torque curve (**Figure 5)** of SS 9, it is worth to understand that at the beginning the rubber phase has got properly dispersed into the TPE matrix and subsequent mixing leads to partial thermal cross-link formation in the rubber phase. But the absence of cross-linker during mixing reduces the cross-linking efficiency as well as the rubber network elasticity (evident from cross-link density value, **Figure 8)** to a great extent which leads to the poor mechanical property obtained for the thermally cross-linked TPVs (SS 9) despite forming of finely dispersed morphology.

Surface topographic images (Figure 10(b)) describe the surface roughness of the concerned TPVs. The root mean square height is found to be 31.1nm from the image analysis. Thus, it can be established that the thermally cross-linked TPV depicts smoother surface finish with poor mechanical property.

3.2.2.2. Scanning Electron Microscopy

Though the AFM images indicate the formation of droplet morphology in case of thermally cross-linked TPV system, but still there was a doubt regarding the poor mechanical property obtained from the thermally cross-linked TPVs. Moreover, several authors have reported that there is an ample chance of co-continuous morphology formation for the 50/50 volume percentage blends if the viscosity ratios are comparable[56, 57]. To investigate these facts further, the cryogenically fractured and etched thermally cross-linked TPV samples were scanned through SEM and the results are given in **Figure 11**. From **Figure 11,** it is evident that the cross-linked rubber phase, which is responsible for droplet morphology formation, has appeared as partially spherical particles in the cross-linked rubbery counterparts. This result is in accord with the AFM observations **(Figure 10(a) and 10(b))**. On the contrary, it also indicates the formation of co-continuous morphology, since the remaining part after the dissolution of the TPE phase is self supporting and the remaining mass fraction after etching is approximately identical with the original mass fraction calculated in the initial TPV[58-60]. Thus, it can be concluded that thermal cross-linking leads to the formation of both co-continuous and droplet morphology in case of S-SBR/S-EB-S blends. It has been further confirmed by adopting Kerner's viscoelastic model and discussed later.

3.3. TPVs containing sulphur Cured Rubber Phase

3.3.1. Mixing Torque and reprocessability of TPVs

Mixing torque gives the idea of shear and elongational flow in actual mixing environment. Mixing has been done following the recipe given in **Table 3** and the mixing torque of the SEV (SST 1) and EV (SST 2) cured TPVs are given in **Figure 3**. Delta torque ($\Delta_{torq.}$) value obtained for EV and SEV cured TPVs are 44.7 Nm and 40.5 Nm respectively. A large increase in torque is observed with the addition of sulphur, indicating the cross-linking of S-SBR elastomer phase. Higher accelerator content (SST 2) results in a stronger increase in mixing torque which suggests a higher cross-link density. The same phenomenon has been proved experimentally and shown later. As shown in **Figure 3**, the mixing torque levels off at the end of dynamic vulcanization, which indicates that the system is still melt processable, even after the formation of cross-linked rubber phase[61]. At this stage, the cross-linked rubber droplets get dispersed in the TPE matrix and due to attainment of higher elasticity, the shear rate acting on it is not high enough to facilitate further break down of the elastic network. Therefore, it eventually ends up with a constant torque level due to the slippage of cross-linked rubber particles at the rotor surface and the chamber wall, while floating into the TPE matrix. The dynamically vulcanized samples were successfully melt-pressed to a thin sheet and correspondingly mechanical **(Table 9)** and dynamic properties have been measured.

3.3.2. Overall c*ross-link density for sulphur cured TPVs by equilibrium solvent swelling method*

Table 9 shows that there is a drastic improvement in elongation at break for the SEV cured TPVs compared to the EV cured ones while maintaining constant tensile strength value after dynamic vulcanization. To understand the phenomenon, the overall cross-link density for both the TPVs has been measured. Results show that there is a 1.05×10^{-5} mol/ml increase in cross-link density (CLD) in case of EV cured TPVs upon dynamic vulcanization (shown in **Figure 12)**. It has been assumed that higher CLD value should improve the tensile strength for the EV cured TPVs followed by a relative reduction in elongation at break compared to the SEV cured systems unlike the results obtained from mechanical properties **(Table 9)**. Thus, it fails to explain the phenomenal improvement in elongation at break for the SEV cured TPVs after dynamic vulcanization. To understand the same, morphology study (SEM) has been conducted and the

results are discussed in the next section (section 3.3.3.1). It is worthy to mention here that the cured S-SBR (S 0) has depicted overall cross-link density value of 1.3×10^{-4} mol/ml which is approximately more than ten times higher than that of the SEV and EV cured TPVs.

3.3.3. Morphology study

3.3.3.1. Scanning Electron Microscopy

To investigate the morphology developed during the TPV formation SEM study has been conducted with the cryogenically fractured and etched specimens and the images are given in **Figure 13(a) and (b) & Figure 13(c) and (d)**. **Figure 13(a) and (b)** represent the SEM images of the SEV cured TPV and **Figure 13(c) and (d)** represent the SEM images of the EV cured TPV. Here again the remaining part after the dissolution of the TPE phase is self supporting and the specimen mass is comparable with the original mass fraction in the initial TPVs[58-60]. Thus, these systems also majorly form co-continuous morphology. Now, magnification of the primary images (**Figure 13(a) and (c)**) reveals another crucial observation for these systems. In **Figure 13(b)** there exists some elongated rubber particles, which are absent in **Figure 13(d).** It is well-known that higher cross-link density is making the rubber phase more elastic in nature. Therefore, in case of EV cured TPV (SST 2) having higher elasticity of the rubber network **(Figure 13(d)),** the shearing action during mixing is not quite enough to achieve the critical stress[62] which may cause the cross-linked (predominantly mono-sulphide linkages of higher bond strength) rubber phase to break up and to attain the droplet-like morphology. In contrary, the SEV cured TPV (SST 1) also fails to achieve the critical stress, but the reduced elasticity of the cross-linked (di-sulphide and poly-sulphide linkages of lower bond strength) rubber network reduces the critical stress value and thus it end-up with co-continuous morphology with elongated rubber particles **(Figure 13(b))**. These morphological observations well agree (139% improvement in elongation at break value for SEV cured TPVs due to the formation of elongated rubber particles) with the mechanical properties obtained for the sulphur cured TPVs given in **Table 9**.

3.3.3.2. Atomic Force Microscopy

To confirm the morphology development during mixing, further investigation has been done with AFM for the sulphur cured TPV systems. **Figure 14(a) and (c)** represent the phase

morphology, whereas, **Figure 14(b) and (d)** depicts surface topography of the SEV cured TPV (SST 1) and EV cured TPV (SST 2) systems respectively. The light yellow images in the phase and topography images represent cross-linked rubber particles, and the brown region represents the TPE phase. From the phase images (**Figure 14(a) and (c))** it is clearly identified that both of the phases are continuous and thus it leads to the formation of co-continuous morphology in both of the TPV systems. On the other hand, the root mean square height obtained from the surface topography (**Figure 14(b) and (d)** is found to be 0.06μm and 0.05μm respectively for SEV cured TPV (SST 1) and EV cured TPV (SST 2) systems which depicts similar surface finish for both of the TPVs.

3.4. Melt rheological study

Complex shear modulus (G^*) as a function of frequency and double strain aptitude at 120°C for TPVs are shown in the **Figure 15(a) and (b)** respectively. From the figures, it can be clearly observed that by increasing frequency the complex shear modulus (G^*) of the TPVs has increased (**Figure 15(a)).** However, the increase is maximum in case of TPV which is EV cross-linked (SST 2), whereas the change in G^* is almost linear for S-SBR vulcanizates (S 0). The frequency-dependence of the modulus is a result of chain and segment mobility in the material. At low frequencies, the polymer chains can follow the applied strain without delay and without loss of energy, because at the terminal zone[63, 64] the enforced chain movements are equal to the applied frequency. With increasing frequencies of the applied strain, entanglements are no longer able to follow the applied strain and they act as temporary cross-links and thus the material shows elasticity. This region of a constant storage modulus and a minimum in loss modulus is called the rubber plateau. Finally at the high frequency, the material has a high modulus, as a result of the rigidity of the polymer chains at these high frequencies. The molecules are not flexible enough to follow the applied strain[65]. Now, S-SBR vulcanizates are well within this rubber plateau zone during the frequency scan and thus the G^* value remains almost unchanged. On the other hand, the TPE (S-EB-S) present in the remaining TPV blends behaves logically as per the theory during the frequency scan, but the presence of cross-linked rubber phase making the responses dissimilar during the frequency scan. Higher cross-link density in the rubber phase makes the TPVs more elastic in nature. Therefore, at high frequency the material becomes rigid and fails to follow the applied strain and thus depicting higher complex modulus (G^*) value.

From **Figure 8** and **Figure 12,** it can be seen that the cross-link density is the highest for SST 2 followed by SST 1 and SS 9 and thus the TPVs are following the same trend during frequency sweep study.

From the theory of strain-dependence of the Payne effect, it is well known that the main contributions to the complex shear modulus (G^*) are the hydrodynamic effect, the polymer network, the filler-polymer and the filler-filler interaction. Since the subjected TPVs and the rubber vulcanizates are devoid of filler particles, therefore the effect of polymer network during the strain sweep for the respective TPVs is shown in **Figure 15(b).** Polymer network formation is a strain-independent contribution of the rubber network and it is the result of the proportionality of the shear modulus to νRT, where ν is the number of moles of elastically effective network chains per unit volume, as a result of vulcanization[66]. This effect can be called as Payne-like effect and from the **Figure 15(b)** it can be clearly observed that the complex shear modulus (G^*) is increasing with the increase in ν value within the dynamic strain range.

For the typical pseudo-plastic materials the complex shear viscosity (η*) decreases as a function of frequency. From **Figure 16** it is evident that initial η* which is proportional to the degree of cross-linking, follows a gradual decreasing trend by increasing frequency, indicating typical pseudo-plastic behavior. Thus, the results again confirm the maximum formation of cross-link-density in case of EV cured TPV (SST 2) followed by SEV cured (SST 1) and thermally cross-linked (SS 9) TPV similar to the overall cross-link density study.

3.5. Dynamic Mechanical Thermal Analysis (DMTA)

Figure 17 represents the temperature dependence of tanδ of pristine polymers i.e. S-SBR vulcanizate (S 0) and S-EB-S (S 1) TPE and the other TPVs e.g. thermally cross-linked TPV (SS 9), SEV cured TPV (SST 1) and EV cured TPV (SST 2) over a temperature range of −100°C to +100°C. For the compounds i.e. S 0 and S 1 the tanδ peaks appear at −4°C and −44°C respectively. However, in case of the TPVs there exists two distinct transition peaks. The first one appearing at lower temperature, which is due to α transition of the soft segments of TPE and the second transition at higher temperature is due to the α transition of the cross-linked rubber phase. Takino et al reported that the usefulness of two tanδ peaks in the temperature distribution curve of loss tangent lies on the individual polymer components exhibiting their own

characteristic properties which are essential to achieve a better magic triangle properties i.e. a good balance between low rolling resistance, high wet grip and high abrasion resistance[67]. **Table 10** demonstrates the elastic modulus, loss modulus and tanδ values at −50°C, 0°C and +50°C for all of the above mentioned polymers[33, 66]. Now, if we compare the transition peaks of S 0 and anyone of the TPVs e.g. SST 2 at around 0°C, then it can be observed that there is a drastic decrease in the tanδ value, which can be explained as follows. In case of rubber vulcanizate (S 0) the entire cross-linked rubber molecules are exposed to the dynamic transition, and it leads to the higher dissipation of energy (higher tanδ value) at the transition zone. But, the addition of TPE reduces the availability of the cross-linked rubber molecules to the dynamic transition. Because the cross-linked rubber phase which remains close to the TPE phase boundary becomes immobilized and thus it cannot contribute to the dynamic transition, and it leads to the lower dissipation of energy (i.e. lower tanδ value). The same argument is valid if the case is for tanδ value drop of TPE soft segment at around −50°C. Like rubber vulcanizate, the damping peak of the pristine TPE, which is relatively higher, reduces drastically for the TPVs. Here again the TPE molecules, which remain close to the interphase, becomes immobilized and thus cannot respond to the dynamic transition[68-70].

It has also been found from **Figure 17** that the damping peaks for the cross-linked rubber phase in case of TPVs has been gradually shifted towards higher temperature with the increase in cross-link density and also there is an increase in tanδ value. This can be explained on the basis of the fact that the increase in cross-link density basically restricts the segmental movement and mobility of the chain segments which leads to an increase in T_g value. Increase in cross-link density also restricts the flow of the TPE phase to penetrate inside the rubber bulk which increases the availability of the cross-linked rubber molecules to the dynamic transition. This means that the possibility of the formation of immobilized elastic rubber domains are getting reduced and thus leading to the increase in the tanδ value for the TPVs having higher cross-link density. Thus, the shift as well as the damping peaks are the highest for the EV cured TPV (SST 2) followed by SEV cured TPV (SST 1) and thermally cross-linked TPV (SS 9), which is also evident from the overall cross-link density study (**Figure 8** and **Figure 12**).

3.6. Predicting the Viscoelastic Behavior of S-EB-S/S-SBR TPVs

To understand the viscoelastic behavior of the subjected TPVs, the existing Kerner model has been applied[71]. In 1956, Kerner introduced the mean field theory to understand the viscoelastic properties of the polymer blends[72, 73]. In this case, Kerner's dispersed phase model and co-continuous phase model have been used to characterize the TPVs. The TPVs were subjected to temperature scan in DMA to obtain the experimental data which has been compared with the theoretical observations. Kerner's two component dispersed phase model for predicting the shear modulus of the polymeric blend is as follows:

$$\frac{G^*}{G_m^*} = \frac{\frac{G_d^*\phi_d}{[(7-5\nu_m)G_m^* + (8-10\nu_m)G_d^*]} + \frac{\phi_m}{15(1-\nu_m)}}{\frac{G_m^*\phi_d}{[(7-5\nu_m)G_m^* + (8-10\nu_m)G_d^*]} + \frac{\phi_m}{15(1-\nu_m)}} \qquad (9)$$

Where, *d* designates the dispersed-phase component, G^* is the complex shear modulus of the TPV, G_m^* is the complex shear modulus of the matrix, G_d^* is the complex shear modulus of the dispersed phase, ν_m is the Poisson ratio of the matrix and ϕ_d and ϕ_m are the volume fraction of the dispersed phase and matrix respectively.

On the other hand, Kerner's co-continuous phase model for predicting the shear modulus is given as:

$$\frac{(G^*-G_1^*)\phi_1}{(7-5\nu)G^* + (8-10\nu)G_1^*} + \frac{(G^*-G_2^*)\phi_2}{(7-5\nu)G^* + (8-10\nu)G_2^*} = 0 \qquad (10)$$

Where, subscripts 1 and 2 represent the parameters for components 1 and 2 respectively.

Poisson ratio (ν) is a temperature dependent function and it has been calculated by Mazich et al.[74] by using the following equation:

$$\nu(T) = 0.17\left[\frac{\log E^*(glass) - \log E^*(T)}{\log E^*(glass) - \log E^*(rubber)}\right] + 0.32 \qquad (11)$$

Where, E^*(glass) and E^*(rubber) are the complex elastic modulus in the glassy and the rubbery regions respectively.

In **Figure 18**, the experimental complex modulus has been plotted over the temperature range from −90°C to +90°C and compared with the theoretically predicted values assuming droplet

morphology (first S-EB-S as matrix and then S-SBR as matrix) as well as co-continuous morphology. It can be seen that below the T_g of the rubber phase, the theoretically predicted values for droplet morphology are deviating from the experimental values, whereas beyond the T_g of the rubber phase, the curves are almost coinciding to each other. This is due to the fact that theoretical prediction via droplet morphology, considering either S-EB-S or S-SBR as matrix, leads the calculations dominated by the matrix phase, because of the wide separation of Tg of the contributing polymers **(Figure 18)**. Therefore, below the Tg of the rubber phase, the complex modulus does not increase like the experimental one considering S-EB-S as matrix.

Similarly, assuming S-SBR as the matrix phase leads to the higher increase in the predicted complex modulus than the experimental values. On the other hand, co-continuous morphology assumes the equal contribution of both of these phases while predicting the complex modulus. Therefore, even at low temperature there exists a similarity between the theoretical and the experimental observations. Thus, it can be concluded that Kerner models predicts co-continuous phase morphology at low temperature range, whereas it predicts a combination of co-continuous and dispersed phase morphology for SS 9 and predominantly co-continuous phase morphology for SST 1 and SST 2 at elevated temperature range which is in accordance with the findings from the morphology study by SEM and AFM.

4. Conclusions

A new binary blend system based on S-EB-S and S-SBR has been reported and its mechanical properties have been measured after varying the S-EB-S proportion to different weight percentage. Based on the result, 50:50 weight percentage of S-EB-S:S-SBR blend has been optimized through DOE. Optimization of processing conditions has been achieved by adopting Taguchi L_9 methodology and ANOVA. From the main effect plot and response table it has been concluded that combination (1-1-1) i.e. 160°C temperature, 60 rpm rotor speed and 10 minutes of mixing time represents the optimum processing conditions considering temperature and rotor speed as the main contributing factors. While performing the optimization tests, thermally cross-linked soft TPVs are derived as a novel by-product and it has been then meticulously characterized by means of FTIR, SEM and AFM for thorough discernment. The end results obtained from DOE are then partially adopted to prepare the soft TPVs based on S-EB-S and S-SBR blends by utilizing sulphur vulcanization technique. Both semi-efficient and efficient

sulphur vulcanization systems (SEV and EV) have been adopted for dynamic vulcanization as the former exhibits better mechanical properties than the latter. Morphological characterization has been conducted through SEM and AFM, and a comparative study has been reported between the three different TPV systems. The formation of dispersed phase morphology is predominant for thermally cross-linked TPVs, where as sulphur cured TPVs adopt co-continuous type of morphology. The formation of co-continuous morphology envisages higher degree of cross-linking for the sulphur cured TPVs and the same has been ascertained through equilibrium solvent swelling study. The mechanical properties also authenticate the morphological and swelling results by depicting higher strength values for the sulphur cured TPVs. The comparative study between the sulphur cured TPVs (SEV and EV) yields better mechanical properties for the SEV cured TPVs due to the formation of elongated rubber particles. These elongated rubber particles, having reduced critical break-down stress value, originates from the melt mixing process due to the presence of di-sulphide and poly-sulphide linkages of lower bond strength. Further, melt rheology study reveals that the complex viscosity (η^*) and complex shear modulus (G^*) increase with the increase in elasticity i.e. the cross-link density of the rubber phase which is corroborated by the morphological observations as well as swelling study. Data reveals that sulphur cured TPVs having higher elasticity of the rubber network depict enhanced η^* and G^* values compared to thermally cross-linked TPVs of reduced elasticity. The temperature scan during dynamic mechanical thermal analysis reveals that the depression of loss tangent ($\tan\delta$) at +50°C is lowest and comparable for SEV and EV cured TPVs compared to thermally cross-linked TPVs. Whereas EV cured TPV depicts highest $\tan\delta$ value at 0°C and lowest at −50°C. These provide qualitative prediction of rolling resistance, wet grip and abrasion resistance of the concerned TPVs while considering their automotive and automotive ancillary applications. Kerner's model of viscoelasticity predicts a combination of co-continuous (major) and dispersed phase (minor) morphology which is in accordance with the morphological observations. Finally it can be affirmed that the newly introduced sulphur vulcanized TPVs based on S-EB-S and S-SBR blends has registered good mechanical property with reduced hardness suitable for static as well as dynamic applications which is a major demerit of many commercial TPV systems and thus opens up a new avenue for the morphology-mechanical-rheological-viscoelastic property correlation in the TPV systems.

5. Acknowledgements

We thank CEAT Limited for the financial support in this work. Thanks to Dr, H. de Groot (Kraton Polymer Research, Belgium) for supplying us free sample of S-EB-S. Finally, we thank Dr. S. Chattopadhyay and Mr. R. K. Bose for their valuable discussion and support.

6. References

1. W. Dierkes, *Journal of Elastomers and Plastics*, 1996, 28, 257-278.
2. W. Dierkes, *Elastomery*, 1999, 1, 18-25.
3. H. J. Manuel and W. Dierkes, *Recycling of Rubber*, RAPRA Review Report no. 99, 9, 3, RAPRA Technology Limited, 1997.
4. J. Karger-Kocsis, in *Polymer blends and alloys*, eds. G. O. Shonaike and G. P. Simon, Marcel Dekker AG, New York, 1999, ch. 5, pp. 125-153.
5. L. A. Utracki, *Polymer Blends Handbook*, Kluwer Academic Publishers, The Netherlands, 2002.
6. U. Wagenknecht, S. Wiessner, G. Heinrich, H. Michael and M. Zichner, *Plastics, Rubber and Composites*, 2006, 35, 393-400.
7. R. M. A. l'Abee, M. van Duin, A. B. Spoelstra and J. G. P. Goossens, *Soft Matter*, 2010, 6, 1758.
8. G. Holden and N. R. Legge, in *Thermoplastic Elastomers*, eds. G. Holden, N. R. Legge, R. P. Quirk and H. E. Schroeders, Hanser, Munich, 1996, ch. 3, pp. 47-50.
9. S. K. De and A. K. Bhowmick, *Thermoplstic elastomers from rubber plastic blends*, Horwood, London, 1990.
10. Akelastomer. http://www.akelastomer.com/eng/eel/pub/products/p_tuftec.html, (accessed January 2014).
11. Polyinsight. http://www.polyinsight.com/contact.htm, (accessed January 2014).
12. M. Bousmina and R. Muller, *Rheologica Acta*, 1996, 35, 369-381.
13. S. Abdou-Sabet, R. C. Puydak and C. P. Rader, *Rubber Chemistry and Technology*, 1996, 69, 476-494.
14. C. F. Antunes, A. V. Machado and M. van Duin, *European Polymer Journal*, 2011, 47, 1447-1459.
15. W. K. Fisher, U.S. Patent 3037954, USA 1962.
16. W. K. Fisher, U.S. Patent 3862106, USA 1973.
17. A. Y. Coran, B. Das and R. P. Patel, U.S. Patent 4130535, USA 1978.
18. A. Y. Coran and R. Patel, *Rubber Chemistry and Technology*, 1980, 53, 141-150.
19. A. Y. Coran, R. P. Patel and D. Williams, *Rubber Chemistry and Technology*, 1982, 55, 116-136.
20. S. Abdou-Sabet, M. A. Fath, U.S. Patent 4311628, USA 1982.
21. A. Mousa, U. S. Ishiaku and Z. A. M. Ishak, *Journal of Applied Polymer Science*, 1998, 69, 1357-1366.
22. R. R. Babu and K. Naskar, *Advances in Polymer Science*, 2011, 239, 219-247.
23. W. Brostow, T. Holjevac Grguric, O. Olea-Mejia, V. Rek and J. Unni, *e-Polymers*, 2008, 8, 355-363.
24. C. Grein, M. Gahleitner and K. Bernreitner, *eXPRESS Polymer Letters*, 2012, 6, 688-696.
25. S. Moritomi, T. Watanabe and S. Kanzaki, *Polypropylene Compounds for Automotive Applications*, Sumitomo Chemical Co. Ltd., 2010.

26. V. Deniz, N. Karakaya and O. G. Ersoy, *Society of Plastics Engineers*, 2009, DOI: 10.1002/spepro.002518, 1-4.
27. P. Sengupta and J. W. M. Noordermeer, *Polymer*, 2005, 46, 12298-12305.
28. W. G. F. Sengers, P. Sengupta, J. W. M. Noordermeer, S. J. Picken and A. D. Gotsis, *Polymer*, 2004, 45, 8881-8891.
29. W. G. F. Sengers, M. Wübbenhorst, S. J. Picken and A. D. Gotsis, *Polymer*, 2005, 46, 6391-6401.
30. Z. Ahmad, K. D. Kumar, M. Saroop, N. Preschilla, A. Biswas, J. R. Bellare and A. K. Bhowmick, *Polymer Engineering & Science*, 2010, 50, 331-341.
31. F. Picchioni, M. Aglietto, E. Passaglia and F. Ciardelli, *Polymer*, 2002, 43, 3323-3329.
32. G. Bayan, U.S. Patent 4927882, USA 1990.
33. B. Lopez, G. Lopitaux, European Patent WO/2011/061145, France 2011.
34. E. A. Murillo and B. L. López, *Macromolecular Symposia*, 2006, 242, 131-139.
35. K. Naskar and J. W. M. Noordermeer, *Rubber Chemistry and Technology*, 2003, 76, 1001-1018.
36. K. Naskar and J. W. M. Noordermeer, *Rubber Chemistry and Technology*, 2004, 77, 955-971.
37. C. Koning, M. Van Duin, C. Pagnoulle and R. Jerome, *Progress in Polymer Science*, 1998, 23, 707-757.
38. P. J. Flory and J. Rehner, *The Journal of Chemical Physics*, 1943, 11, 512.
39. L. Mullins and N. R. Tobin, *Journal of Applied Polymer Science*, 1965, 9, 2993-3009.
40. T. Chatterjee, S. Wiessner, K. Naskar and G. Heinrich, *eXPRESS Polymer Letters*, 2013, 8, 220-231.
41. R. R. Babu, N. K. Singha and K. Naskar, *Journal of Polymer Research*, 2010, 18, 31-39.
42. R. R. Babu, N. K. Singha and K. Naskar, *eXPRESS Polymer Letters*, 2008, 2, 226-236.
43. M. Barlkanl and C. Hepburn, *Iranian Journal of Polymer Science & Technology*, 1992, 1, 1-5.
44. H. Dikland, Ph.D. Thesis, University of Twente, The Netherlands, 1992.
45. R. K. Roy, *Design of Experiments Using The Taguchi Approach: 16 Steps to Product and Process Improvement*, John Wiley and Sons, New York, 2001.
46. A. Salahi, T. Mohammadi, M. Nikbakht, M. Golshenas and I. Noshadi, *Desalination and Water Treatment*, 2012, 48, 27-37.
47. M. S. Sureshkumar, K. Naskar, G. B. Nando, Y. K. Bhardwaj and S. Sabharwal, *Polymer-Plastics Technology and Engineering*, 2008, 47, 341-345.
48. S. Mohapatra and G. B. Nando, *RSC Advances*, 2014, 4, 15406-15418.
49. R. Giri, K. Naskar and G. B. Nando, *Plastics, Rubber and Composites*, 2012, 41, 341-349.
50. Y. Ma, H. Hu, D. Northwood and X. Nie, *Journal of Materials Processing Technology*, 2007, 182, 58-64.
51. F. Goharpey, A. A. Katbab and H. Nazockdast, *Journal of Applied Polymer Science*, 2001, 81, 2531-2544.
52. C. F. Antunes, M. van Duin and A. V. Machado, *Materials Chemistry and Physics*, 2012, 133, 410-418.
53. J. A. Gopi and G. B. Nando, *Journal of Elastomers and Plastics*, 2011, 44, 189-204.
54. D. R. Paul and C. B. Bucknall, *Polymer Blends: Formulation*, John Wiley and Sons, New York, 2000.

55. G. Socrates, *Infrared and Raman Characteristic Group Frequencies: Tables and Charts*, John Wiley and Sons, Bristol, 2004.
56. D. R. Paul and J. W. Barlow, *Journal of Macromolecular Science, Part C: Polymer Reviews*, 1980, 18, 109-168.
57. G. M. Jordhamo, J. A. Manson and L. H. Sperling, *Polymer Engineering & Science*, 1986, 26, 517-524.
58. F. Gubbels, S. Blacher, E. Vanlathem, R. Jerome, R. Deltour, F. Brouers and P. Teyssie, *Macromolecules*, 1995, 28, 1559-1566.
59. P. Pötschke and D. R. Paul, *Journal of Macromolecular Science, Part C*, 2003, 43, 87-141.
60. C. Lagrève, J. F. Feller, I. Linossier and G. Levesque, *Polymer Engineering & Science*, 2001, 41, 1124-1132.
61. Y. Li, Y. Oono, Y. Kadowaki, T. Inoue, K. Nakayama and H. Shimizu, *Macromolecules*, 2006, 39, 4195-4201.
62. R. M. A. l'Abee, Ph.D. Thesis, Eindhoven University of Technology, The Netherlands, 2009.
63. K. P. Menard, *Dynamic Mechanical Analysis: A Practical Introduction*, Boca Raton LLC, Florida, 1999.
64. S. Hui, T. K. Chaki and S. Chattopadhyay, *Polymer Composites*, 2010, 31, 377-391.
65. W. K. Dierkes, Ph.D. Thesis, University of Twente, The Netherlands, 2005.
66. A. t. Brinke, Ph.D. Thesis, University of Twente, The Netherlands, 2002.
67. H. Takino, S. Iwama, R. Ohara, N. Isobe, H. Tobori, M. Komai, U.S. Patent 4946887, USA 1990.
68. N. G. McCrum, *Journal of Polymer Science*, 1958, 27, 555-558.
69. A. Jha and A. K. Bhowmick, *Rubber Chemistry and Technology*, 1997, 70, 798-814.
70. S. S. Banerjee and A. K. Bhowmick, *Polymer*, 2013, 54, 6561-6571.
71. D. R. Paul and S. Newman, *Polymer blends*, Academic Press, New York, 1978.
72. E. H. Kerner, *Proc. Phys. Soc. B*, 1956, 69, 808-813.
73. G. G. Bandyopadhyay, S. S. Bhagawan, K. N. Ninan and S. Thomas, *Journal of Polymer Science Part B: Polymer Physics*, 2004, 42, 1417-1432.
74. K. A. Mazich, H. K. Plummer, M. A. Samus and P. C. Killgoar, *Journal of Applied Polymer Science*, 1989, 37, 1877-1888.

Figures Captions

- Figure 1. Microscopic images of (a) TPE[10] and (b) TPV[11]
- Figure 2. Two dimensional polymeric structures of (a) S-SBR rubber and (b) S-EB-S thermoplastic elastomer.
- Figure 3. Torque-Time curves for S-EB-S/S-SBR TPVs (SEV and EV systems)
- Figure 4. Plot of (a) tensile strength and (b) elongation at break versus S-EB-S (wt%) for the S-EB-S/S-SBR blends.
- Figure 5. Torque-Time curves for S-EB-S/S-SBR blends as per Taguchi compositions
- Figure 6. Main effects plot for SN ratios of S-EB-S/S-SBR blends for (a) tensile strength and (b) elongation at break.
- Figure 7. Interaction plots for design parameters (a) tensile strength and (b) elongation at break.
- Figure 8. Cross-link density for thermally cross-linked Taguchi blends
- Figure 9. Infrared spectra of SS 1 and SS 9 showing the peaks in the range from 1800-1500 cm^{-1}
- Figure 10. AFM (a) phase images, (b) surface topography and (c) particle size distribution plot for thermally cross-linked TPVs [scan area 10×10 μm^2].
- Figure 11. SEM Images of thermally cross-linked S-EB-S and S-SBR TPVs after solvent etching at the magnification of (a) 150× and (b) 500×.
- Figure 12. Overall cross-link density for SEV (SST 1) and EV (SST 2) cured TPVs.
- Figure 13. SEM images of sulphur cured S-EB-S and S-SBR TPVs after solvent etching: (a) and (b) SEV cured TPVs at 500× and 3000× magnifications and (c) and (d) EV cured TPVs at 500× and 3000× magnifications respectively.
- Figure 14. AFM phase images (a) and (c) and surface topography (b) and (d) of SEV cured TPV and EV cured TPV respectively [scan area 10×10 μm^2].
- Figure 15. Variation of complex modulus (G^*) as a function of (a) frequency and (b) strain amplitude of dynamically vulcanized blends and rubber vulcanizate.
- Figure 16. Variation of complex shear viscosity (η^*) as a function of frequency of dynamically vulcanized blends and rubber vulcanizate.

- Figure 17. Temperature dependence of loss tangent (tanδ) of dynamically vulcanized blends, rubber vulcanizate and pristine TPE.
- Figure 18. Experimental and theoretical plots of complex shear modulus (G^*) of (a) thermally cross-linked, (b) SEV cured and (c) EV cured TPVs using Kerner's dispersed and co-continuous phase models.

Tables Captions

- Table 1 - Factors and levels designed for S-EB-S and S-SBR (50:50) blends
- Table 2 - Experimental layout based on Taguchi L_9 model
- Table 3: Compounding recipe of S-EB-S/ S-SBR TPVs (In phr*)
- Table 4 – Mechanical properties of EB 2, i.e. 50:50 S-EB-S/S-SBR blends as per Taguchi L_9 methodology
- Table 5: Response Table for Signal to Noise Ratios - Higher is better (Tensile Strength)
- Table 6: Response Table for Signal to Noise Ratios - Higher is better (Elongation at Break)
- Table 7: Response Table for ANOVA analysis (TS)
- Table 8: Response Table for ANOVA analysis (EB)
- Table 9 – Mechanical properties of sulphur cured TPVs (Standard deviation values for five numbers of test specimen are given in parenthesis)
- Table 10: Dynamic mechanical properties of TPVs, rubber vulcanizate and pristine TPE

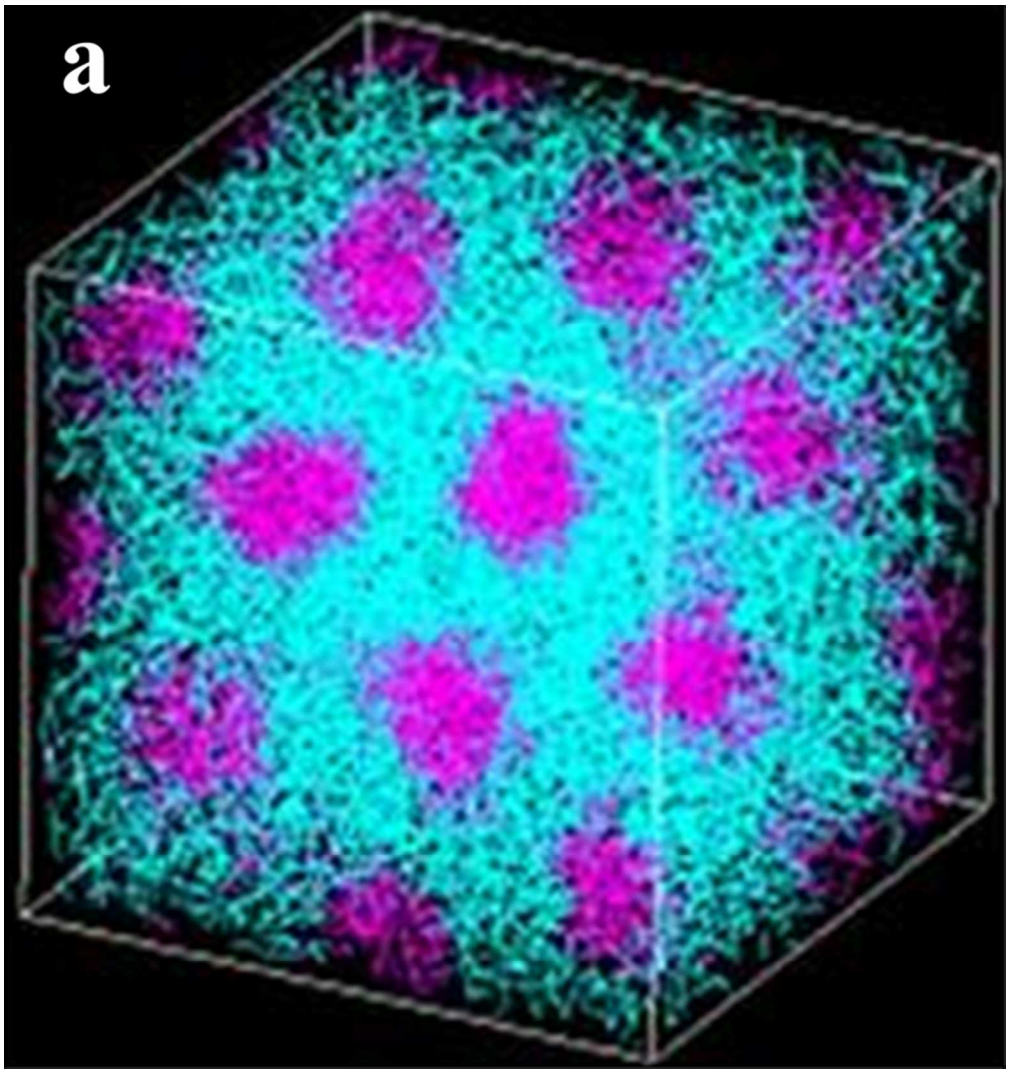

1(a)
79x84mm (275 x 275 DPI)

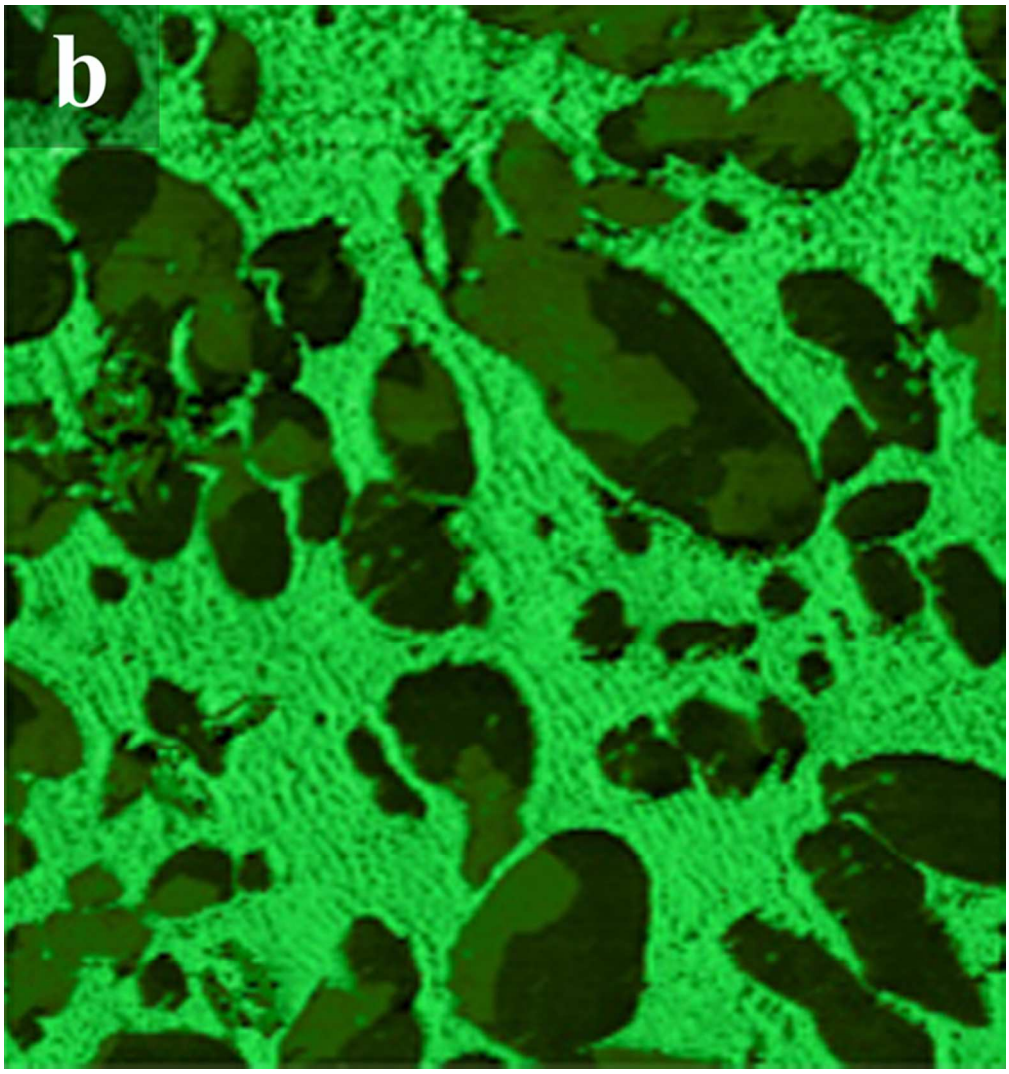

1(b)
79x84mm (275 x 275 DPI)

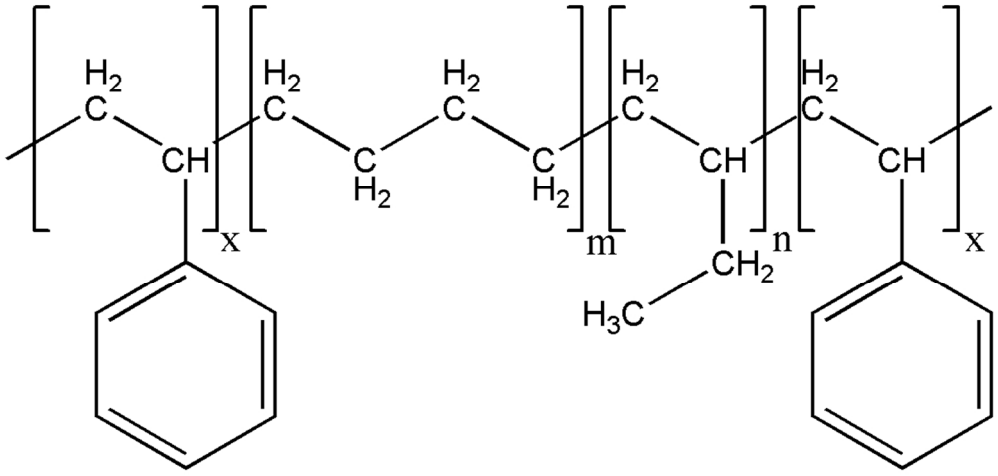

2(a)
102x49mm (300 x 300 DPI)

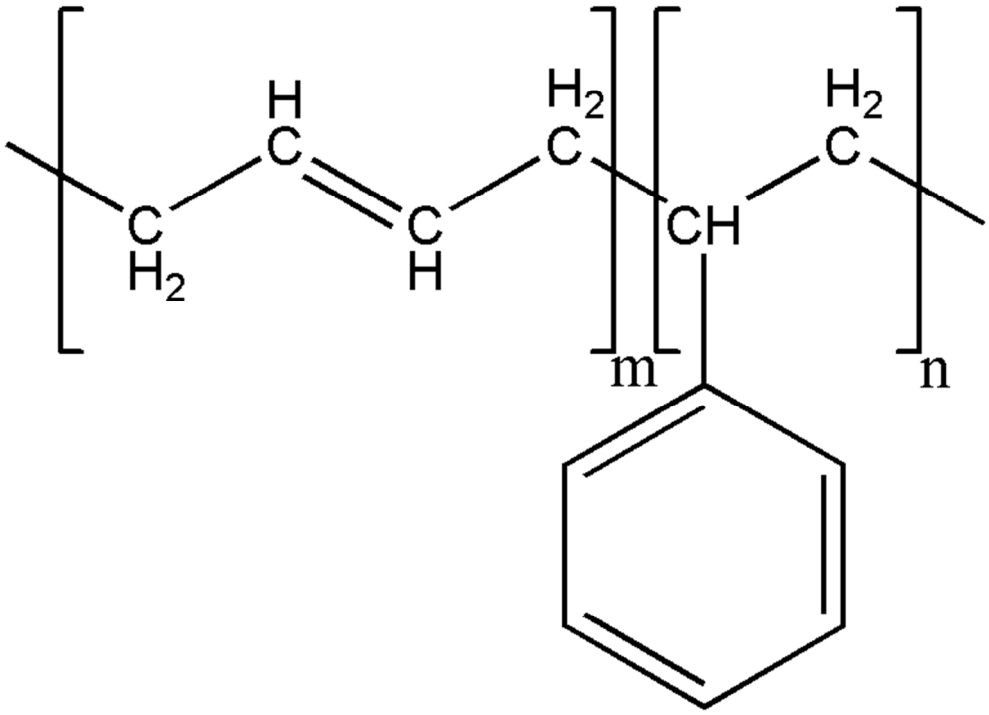

2(b)
65x48mm (300 x 300 DPI)

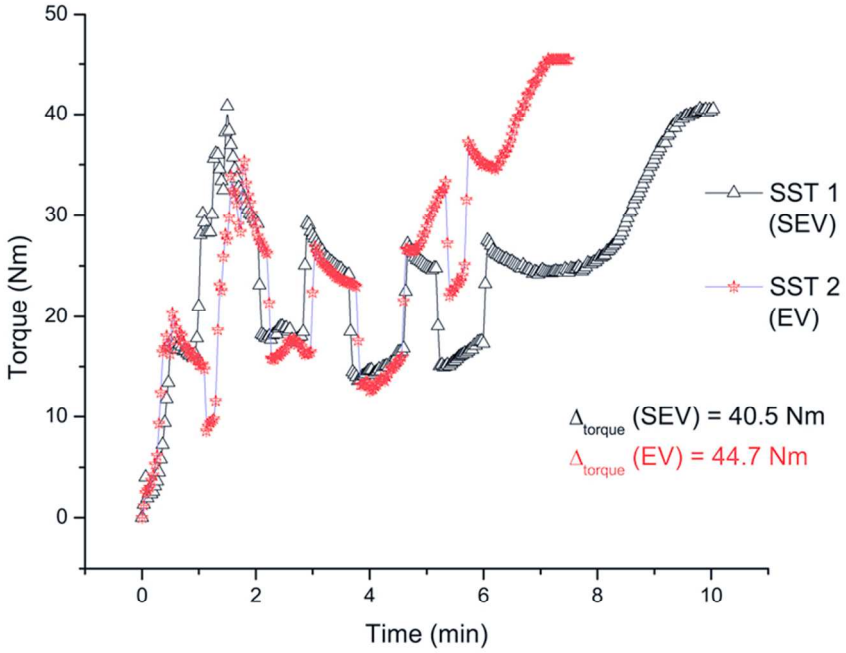

3
80x61mm (300 x 300 DPI)

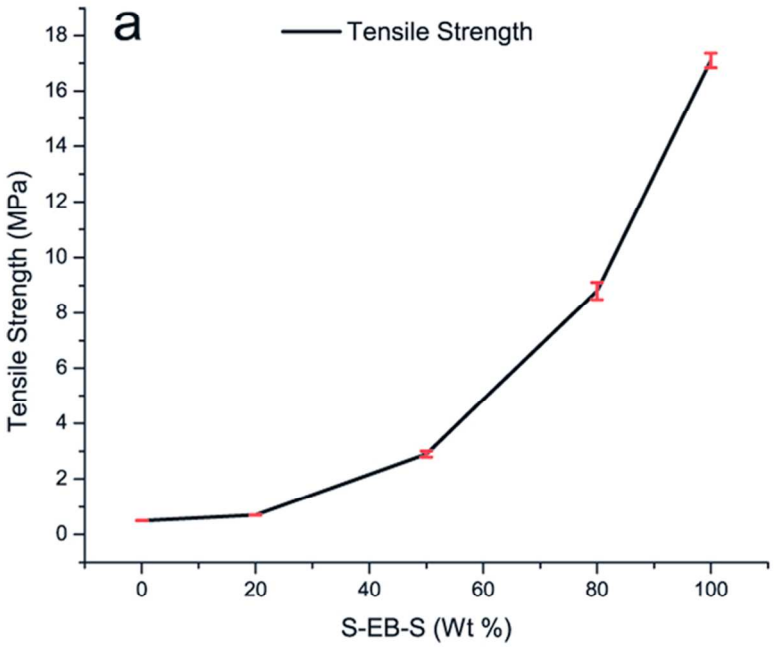

4(a)
80x61mm (300 x 300 DPI)

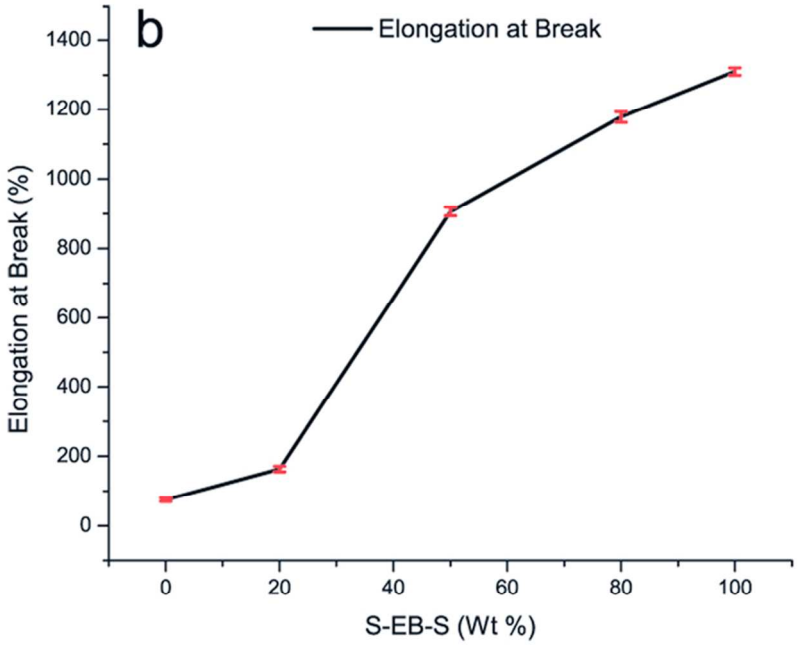

4(b)
80x61mm (300 x 300 DPI)

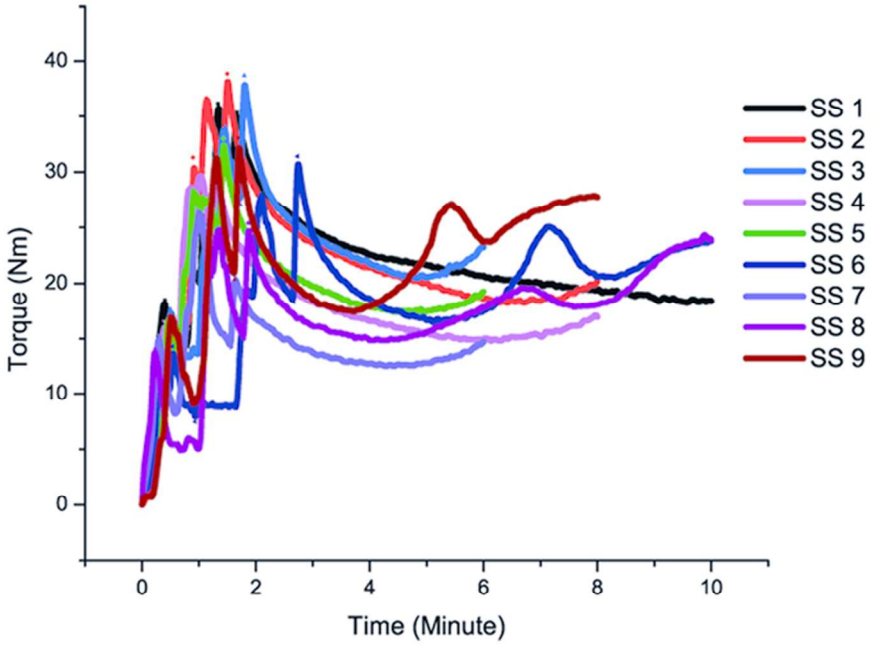

5
80x61mm (300 x 300 DPI)

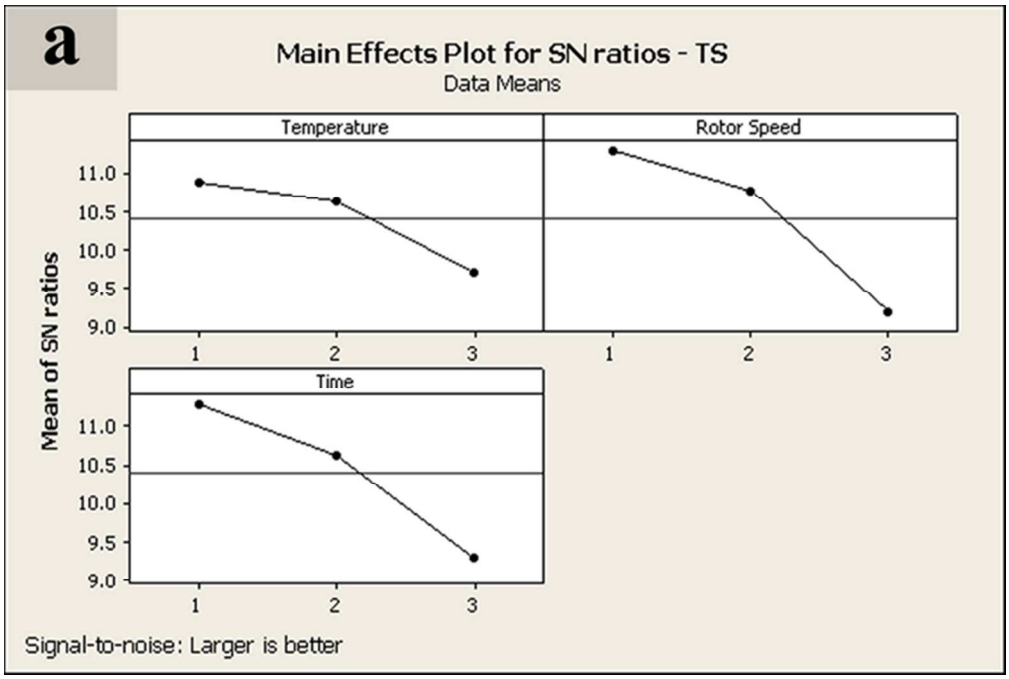

6(a)
79x53mm (250 x 250 DPI)

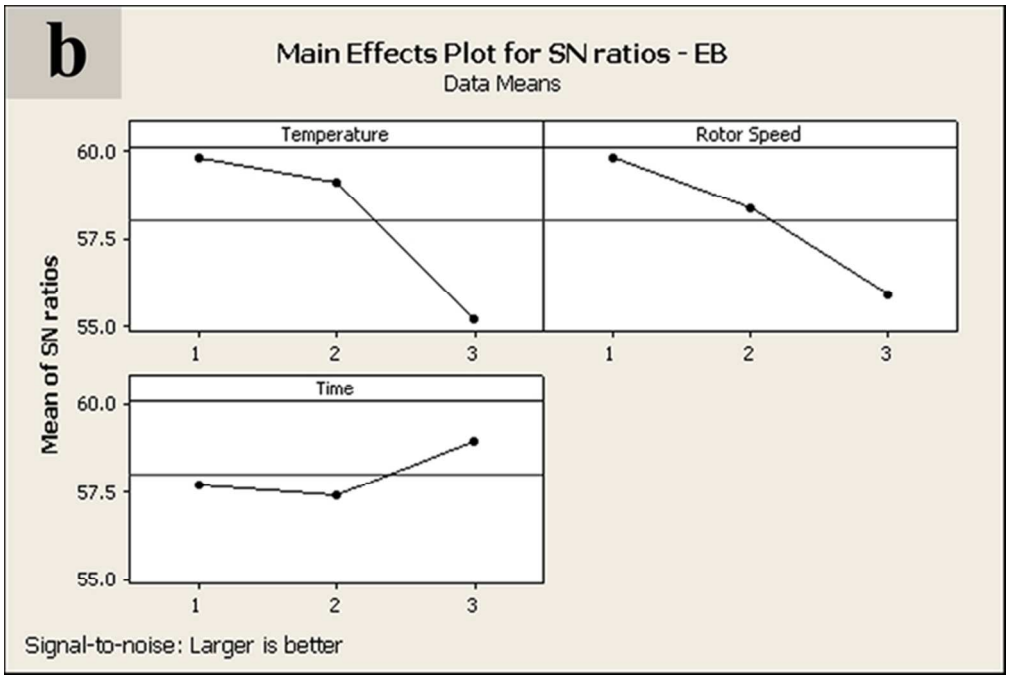

6(b)
79x53mm (250 x 250 DPI)

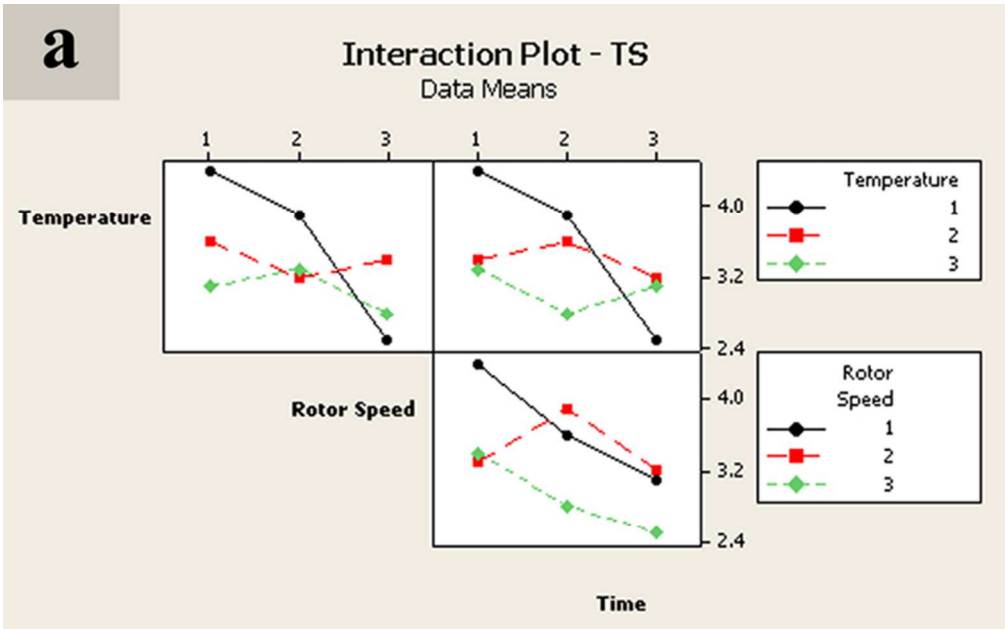

7(a)
79x49mm (250 x 250 DPI)

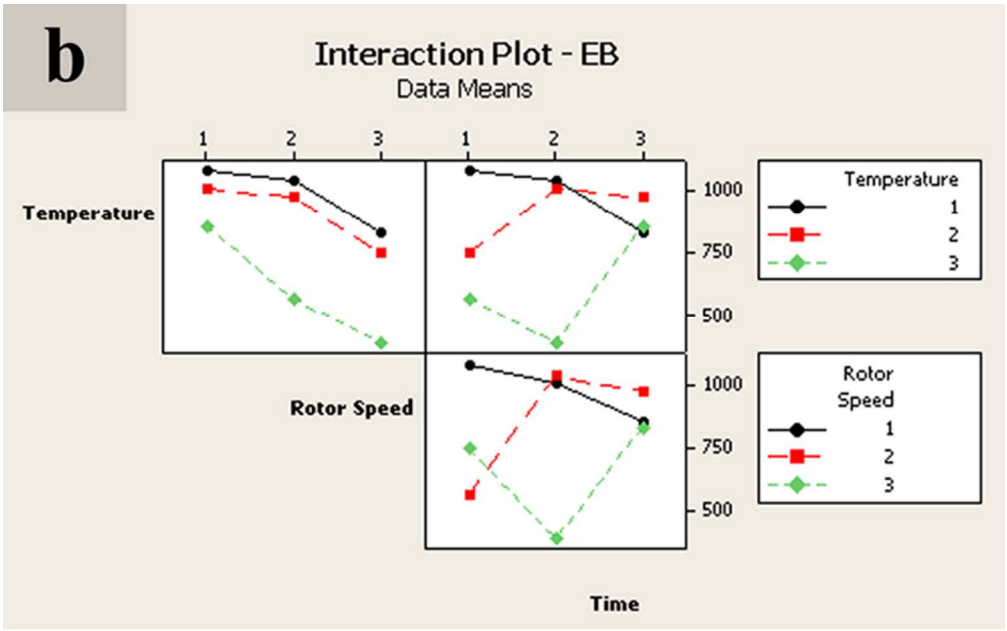

7(b)
79x49mm (250 x 250 DPI)

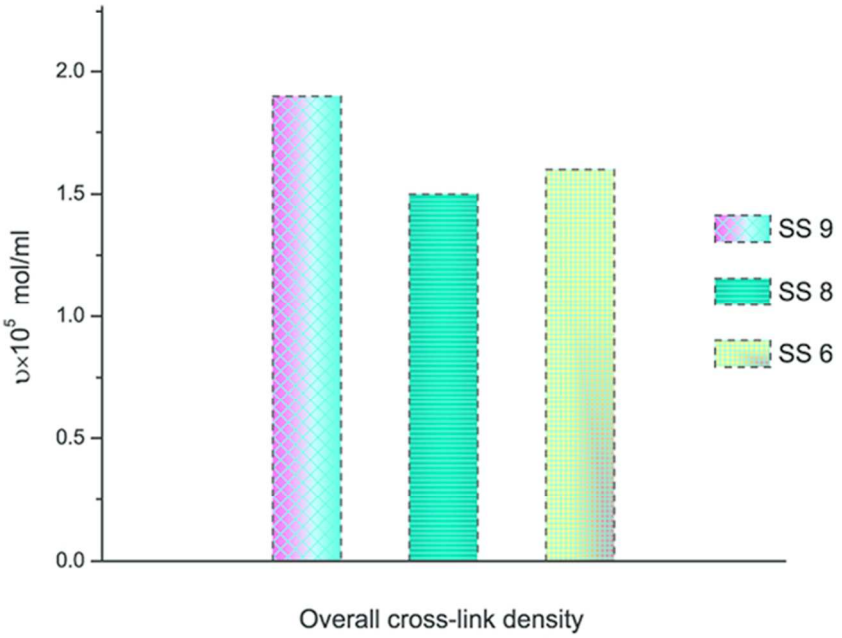

8
80x61mm (300 x 300 DPI)

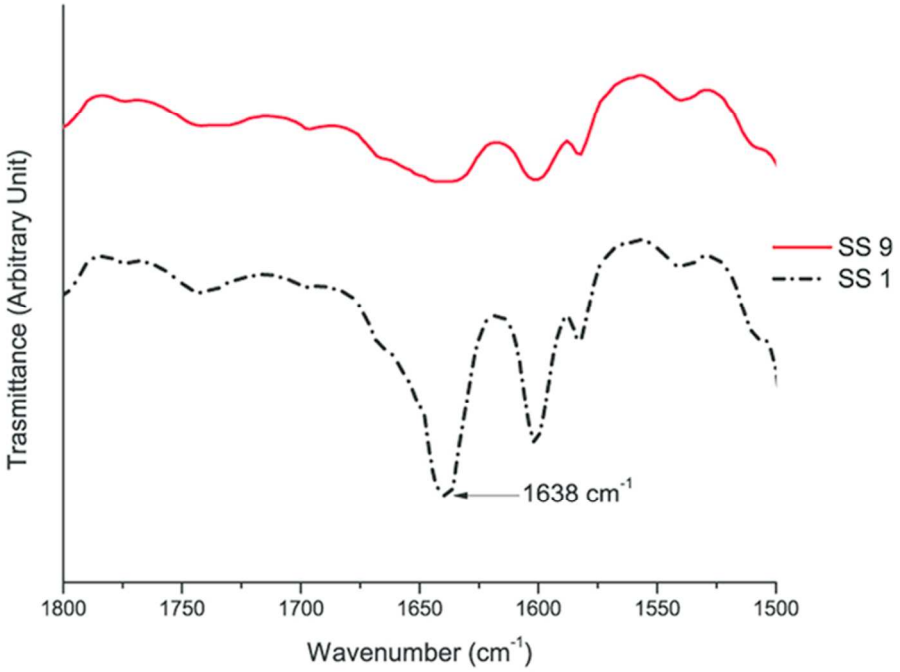

9
80x61mm (300 x 300 DPI)

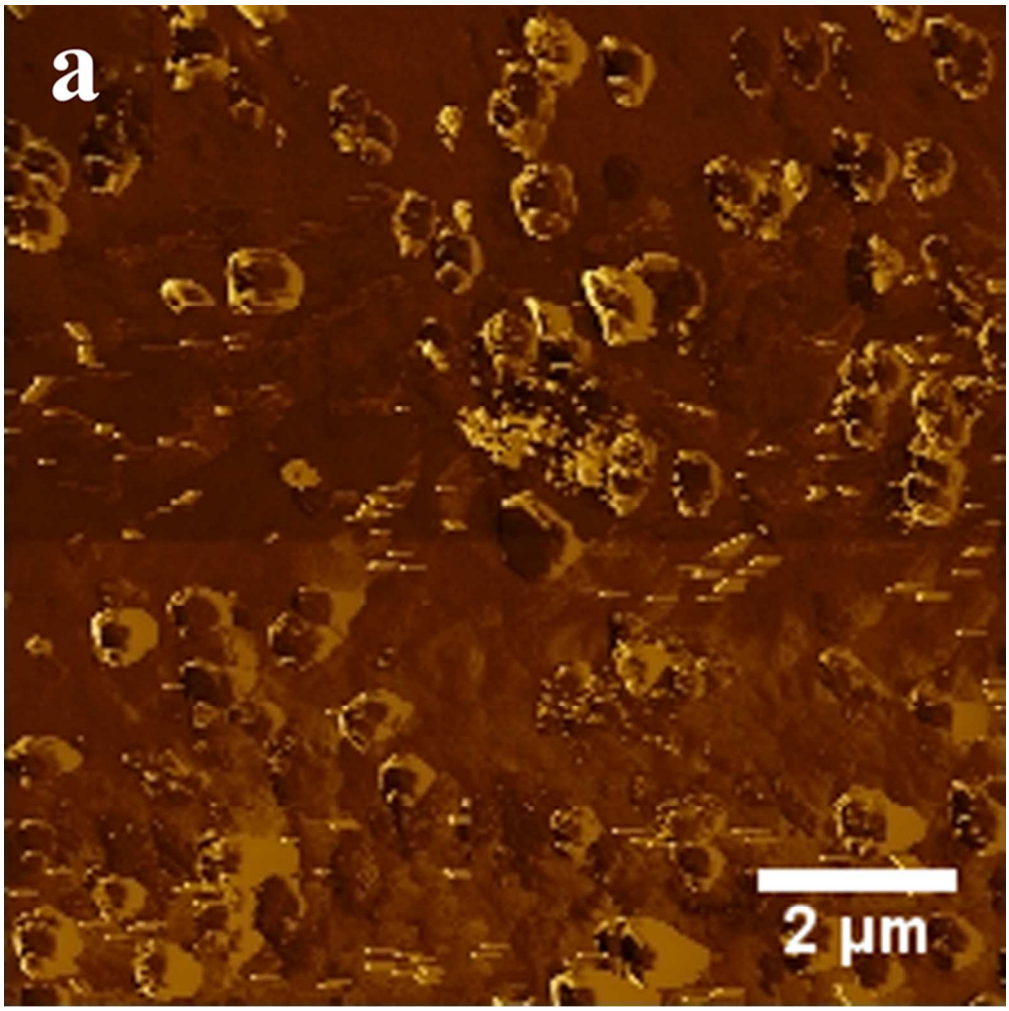

10(a)
79x79mm (250 x 250 DPI)

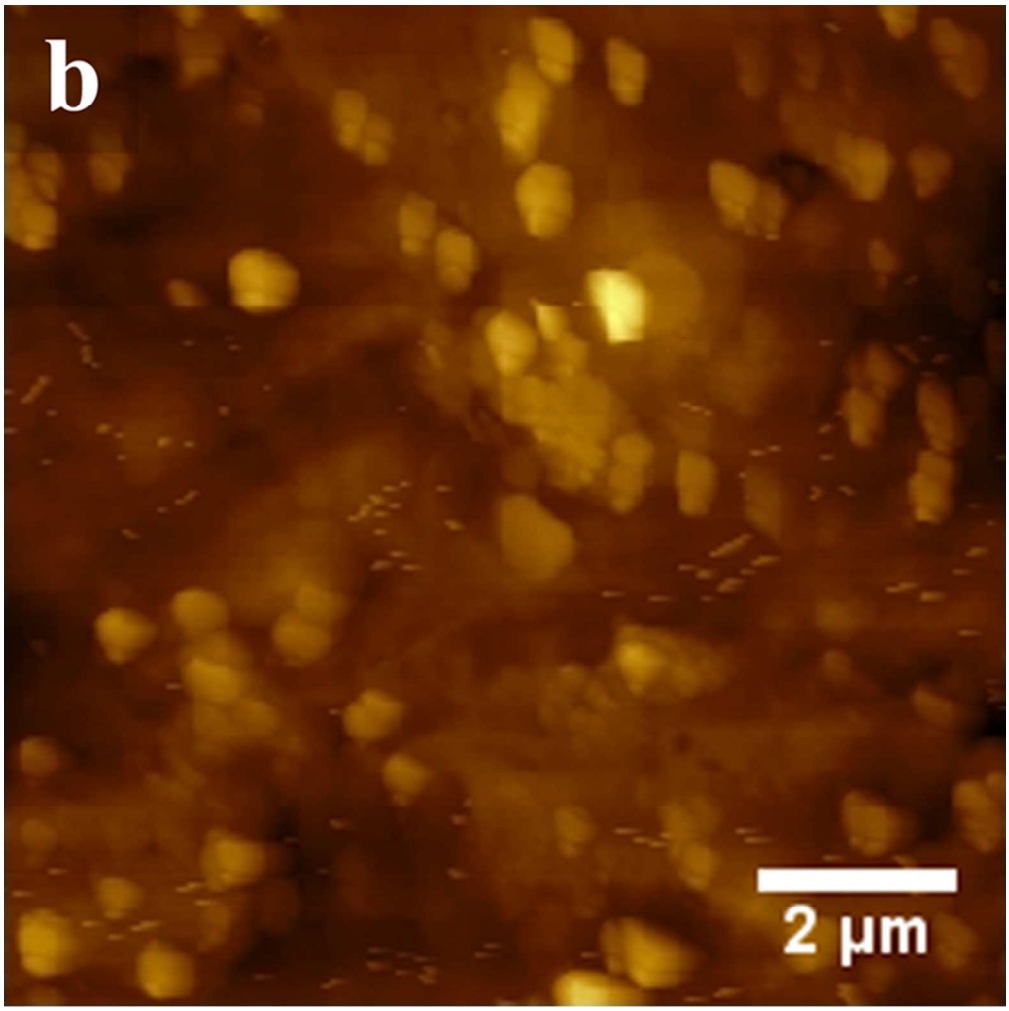

10(b)
79x79mm (250 x 250 DPI)

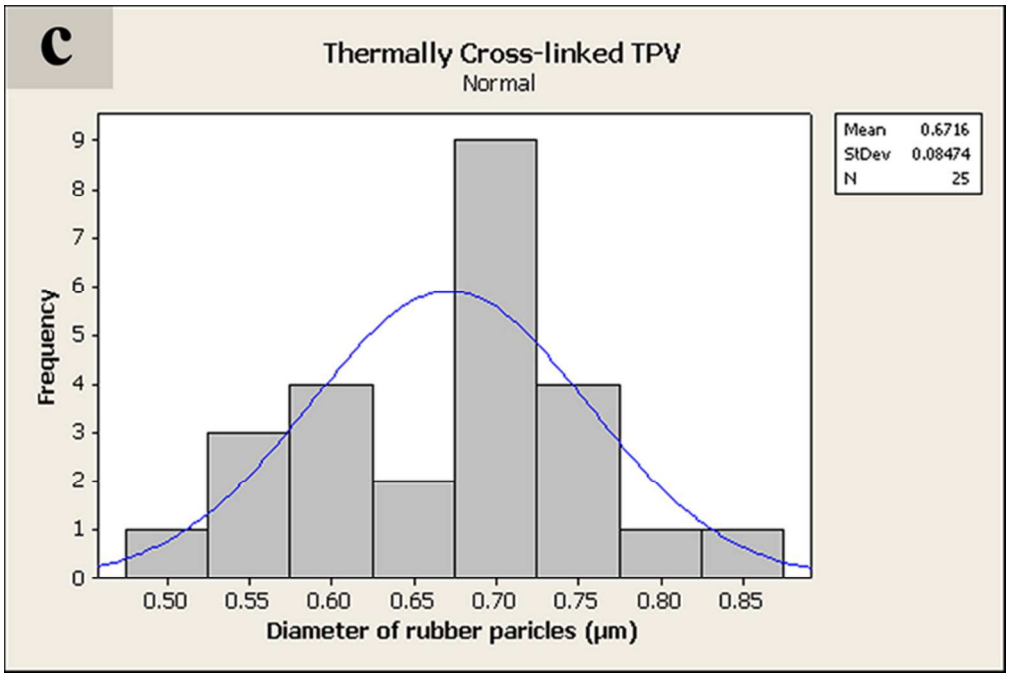

10(c)
79x53mm (250 x 250 DPI)

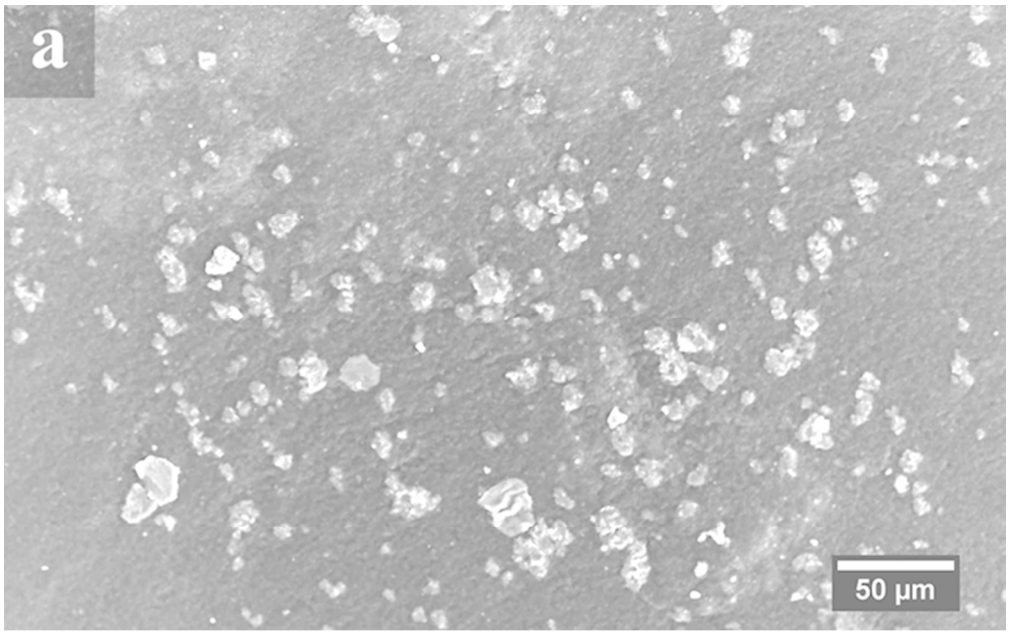

11(a)
79x49mm (250 x 250 DPI)

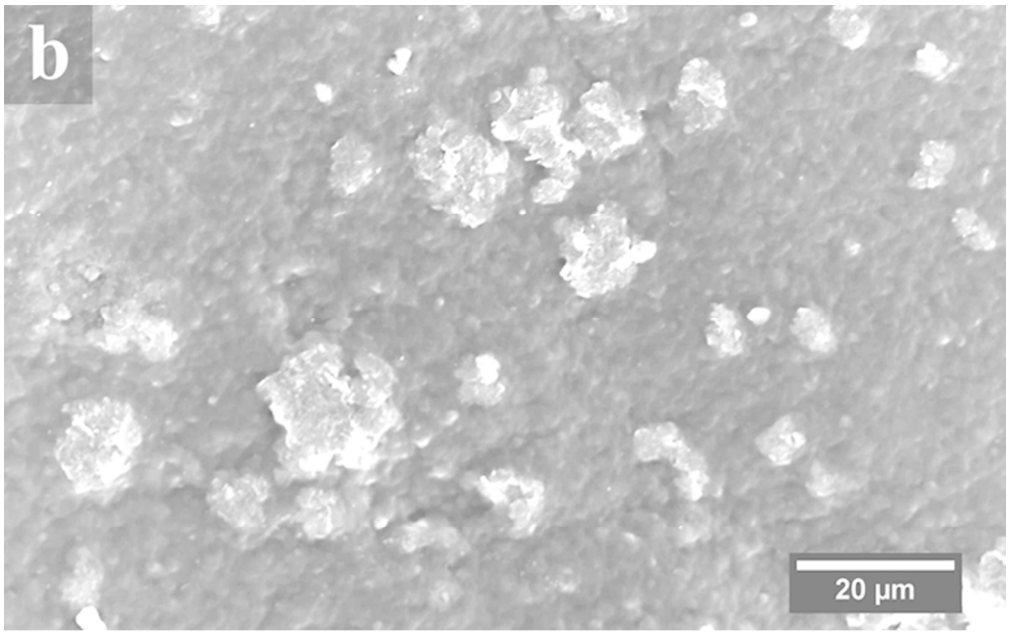

11(b)
79x49mm (250 x 250 DPI)

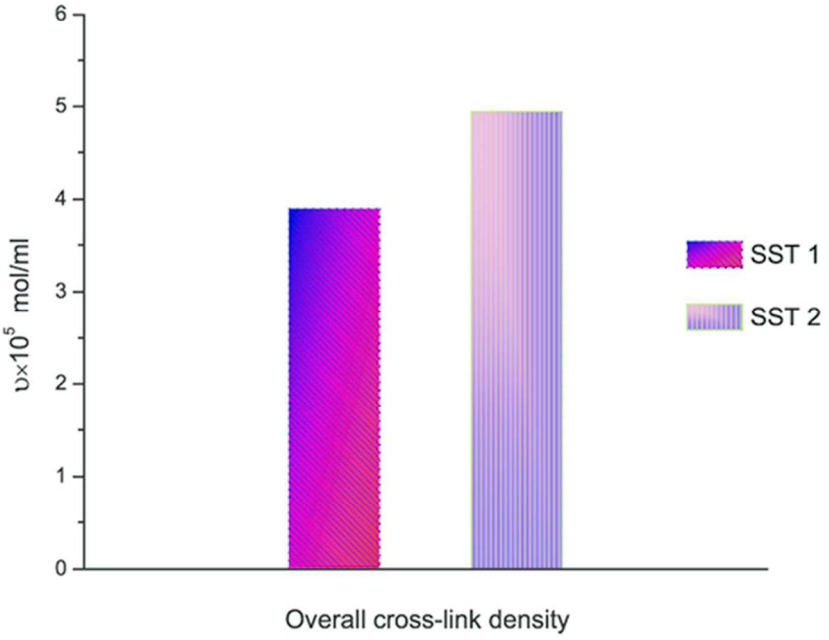

12
80x61mm (300 x 300 DPI)

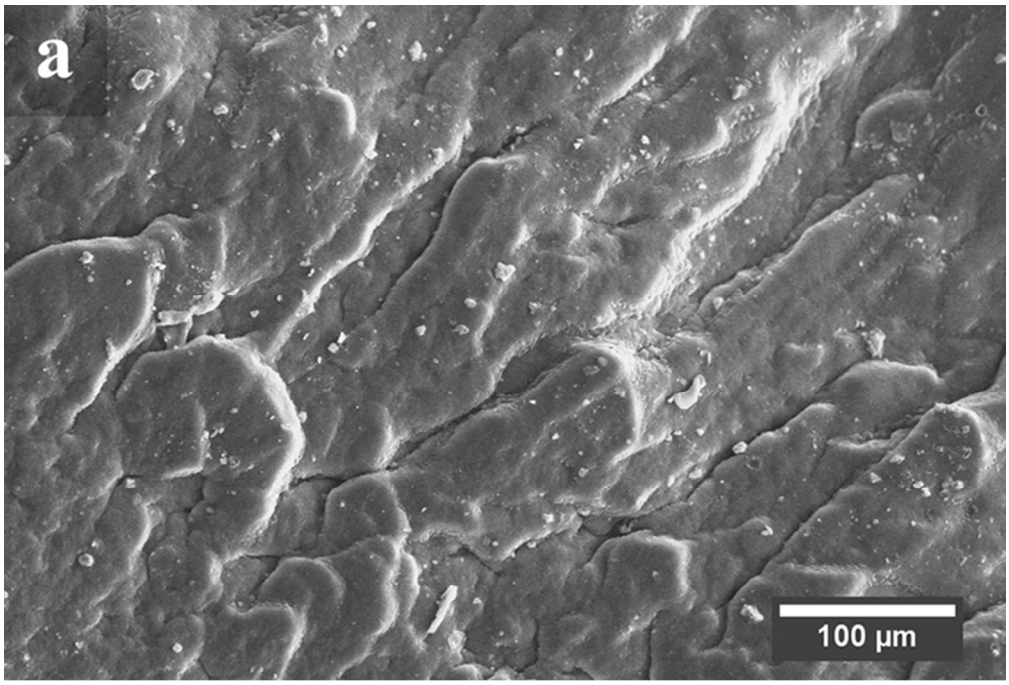

13(a)
79x53mm (250 x 250 DPI)

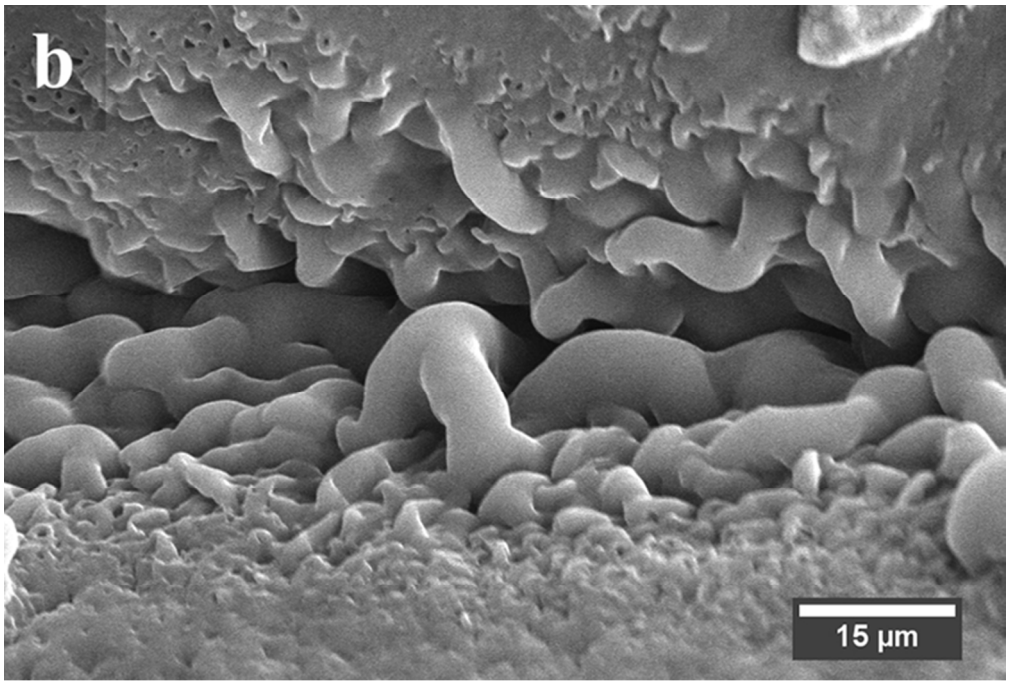

13(b)
79x53mm (250 x 250 DPI)

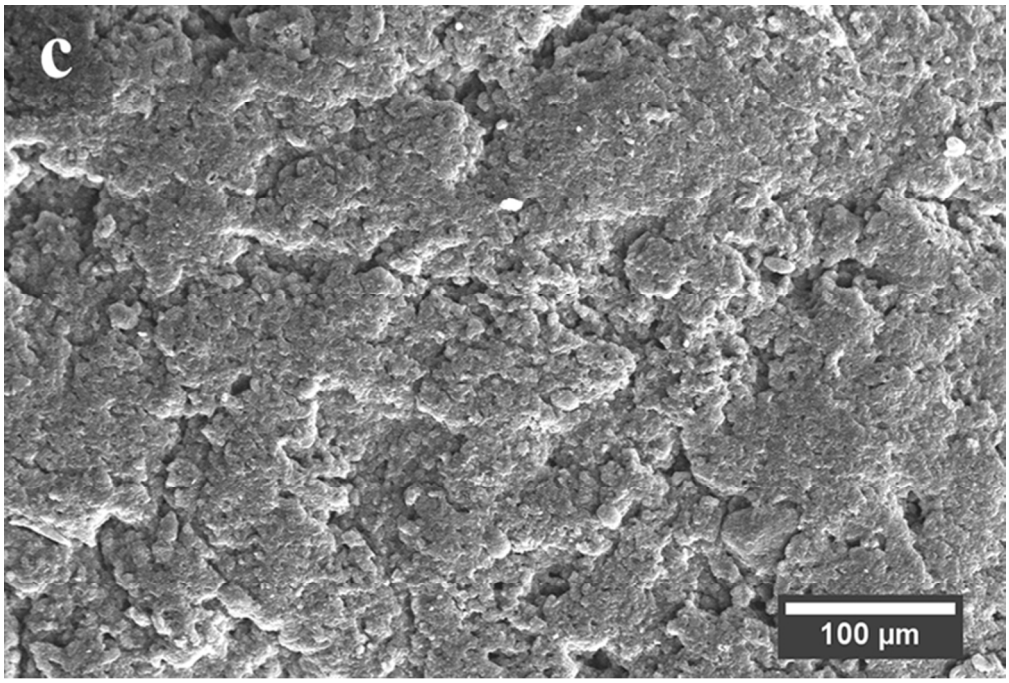

13(c)
79x53mm (250 x 250 DPI)

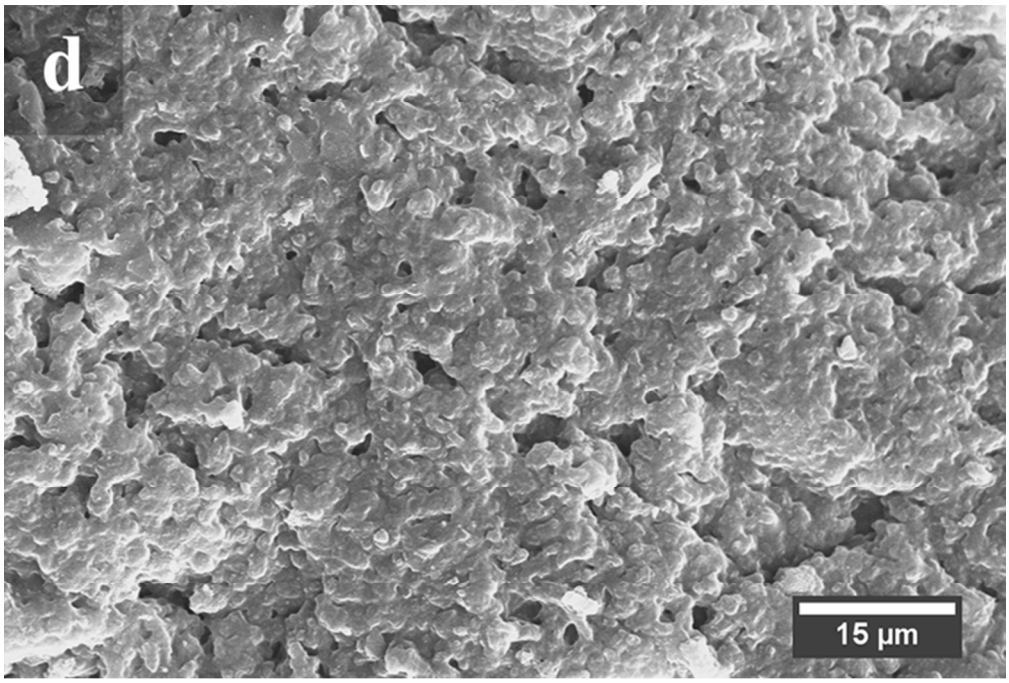

13(d)
79x53mm (250 x 250 DPI)

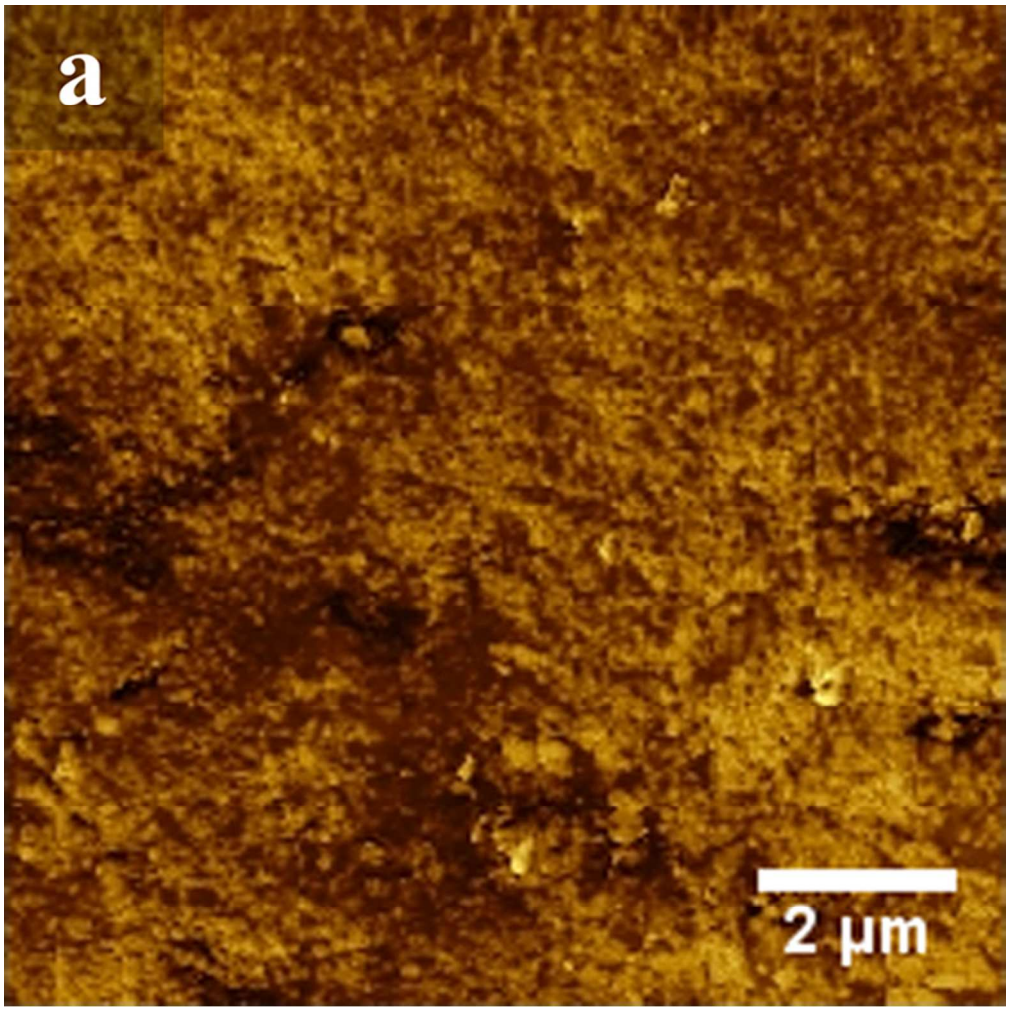

14(a)
79x79mm (250 x 250 DPI)

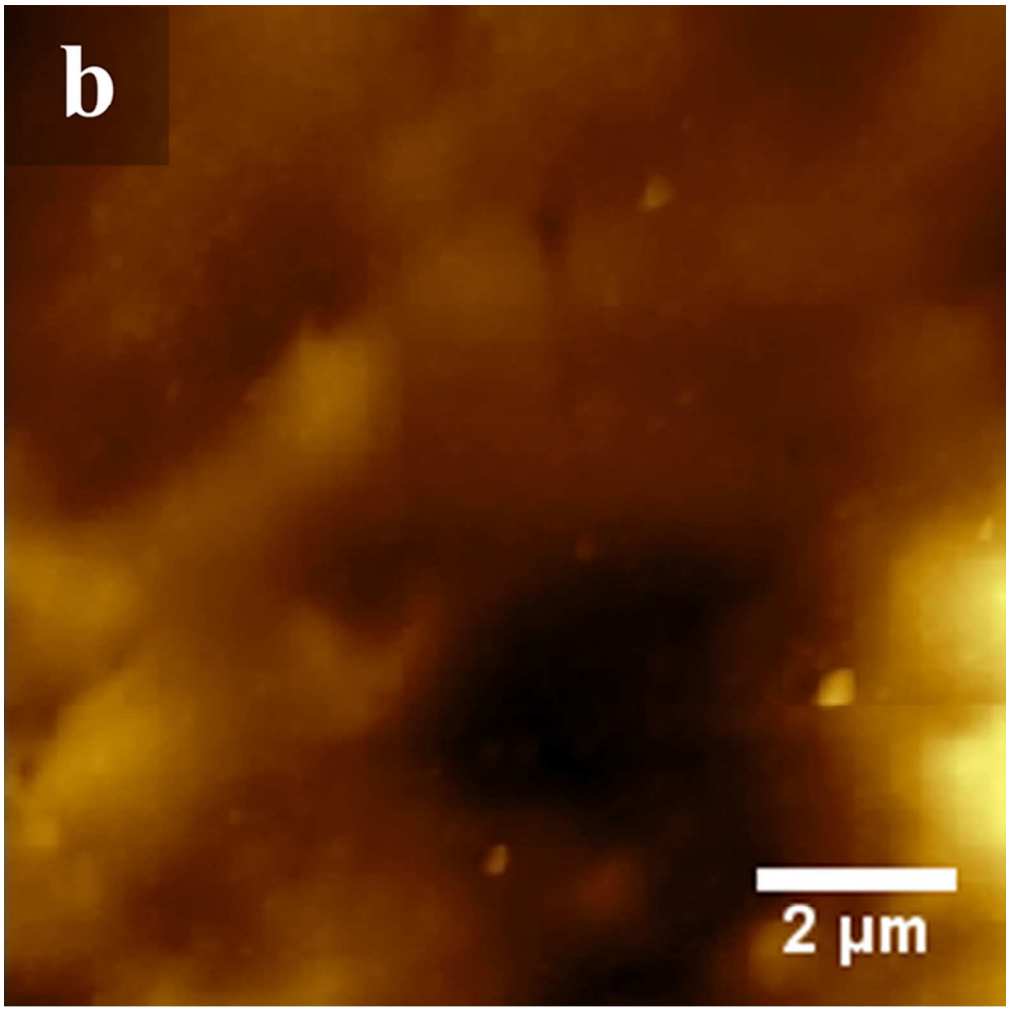

14(b)
79x79mm (250 x 250 DPI)

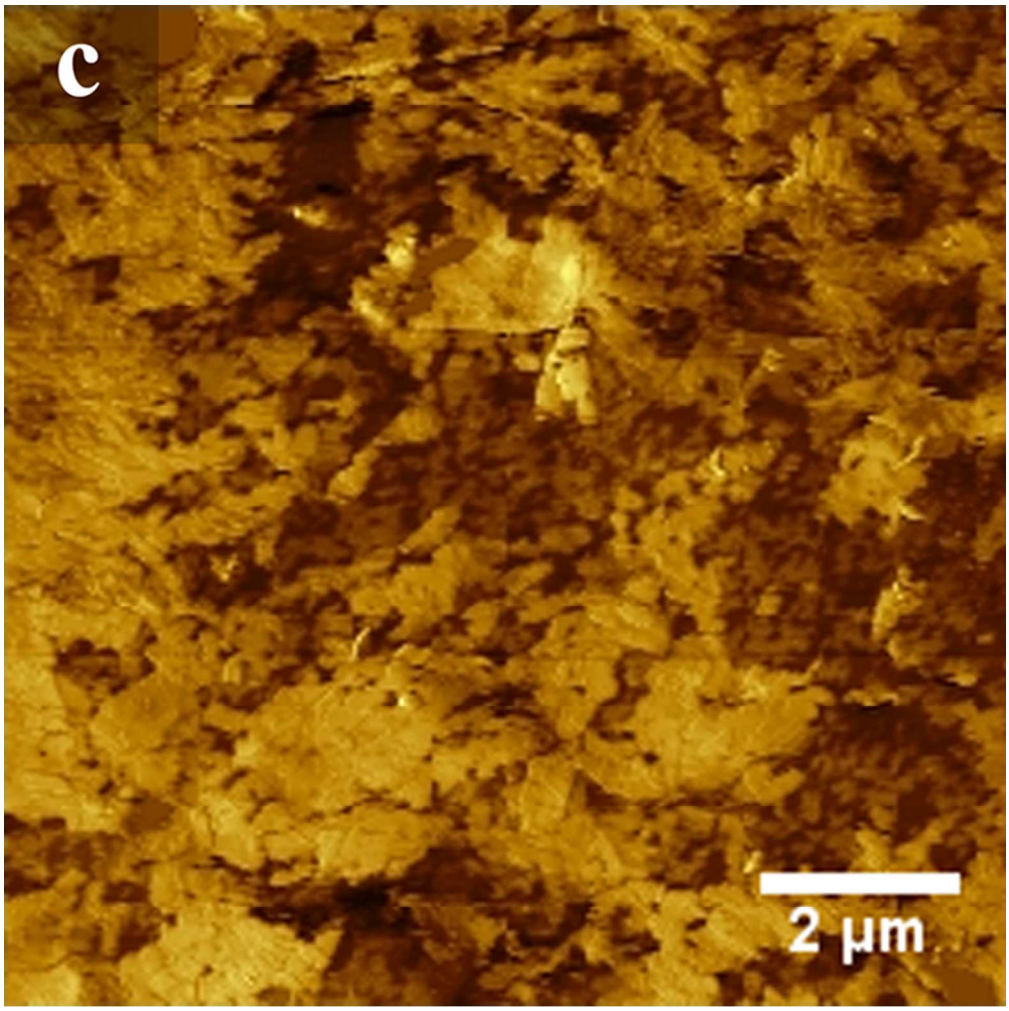

14(c)
79x79mm (250 x 250 DPI)

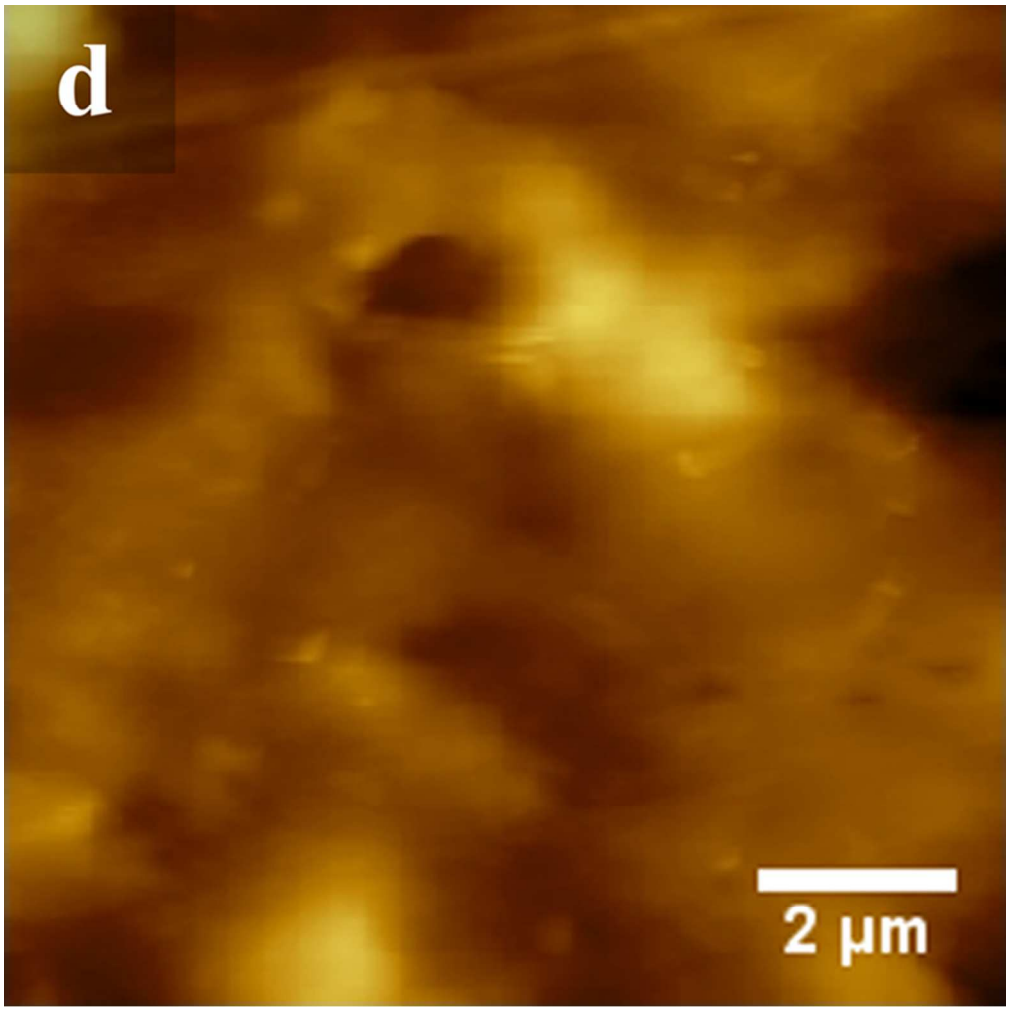

14(d)
79x79mm (250 x 250 DPI)

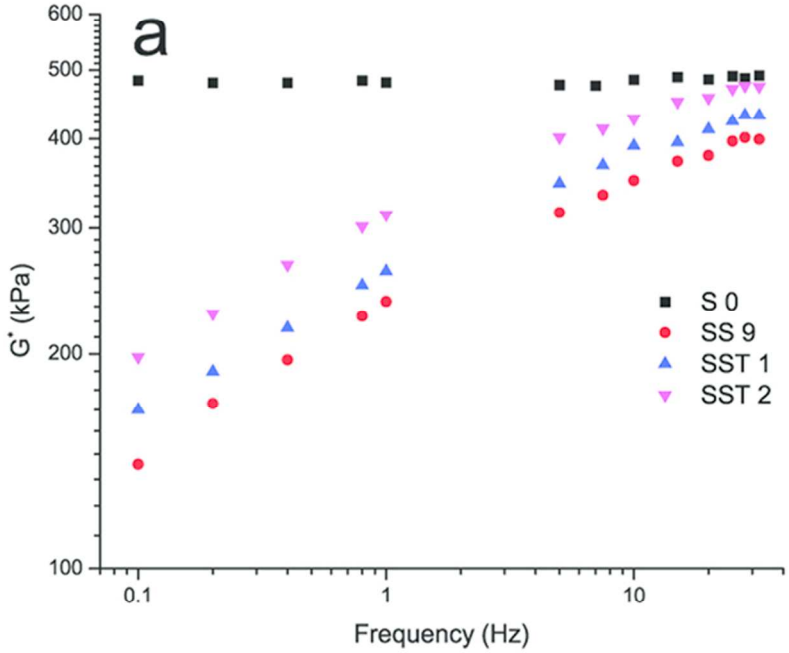

15(a)
80x61mm (300 x 300 DPI)

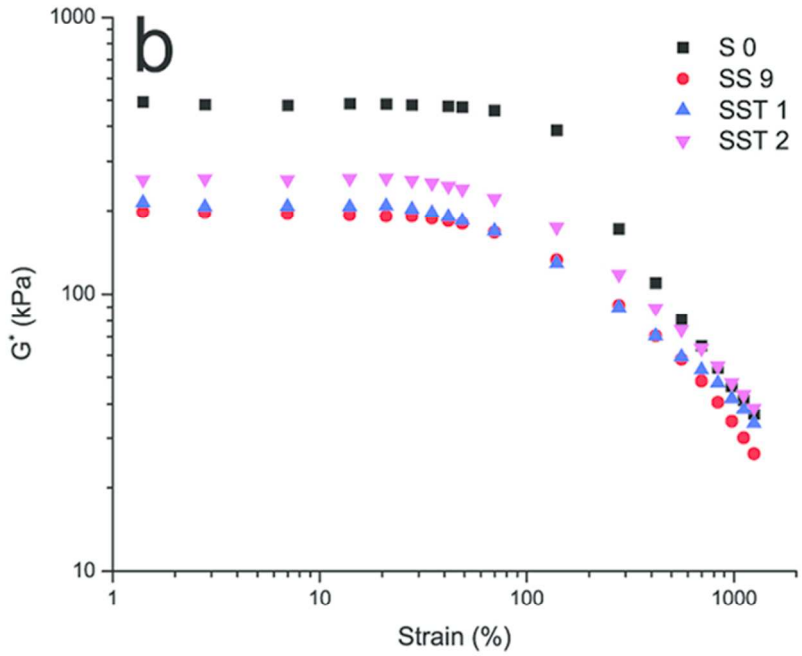

15(b)
80x61mm (300 x 300 DPI)

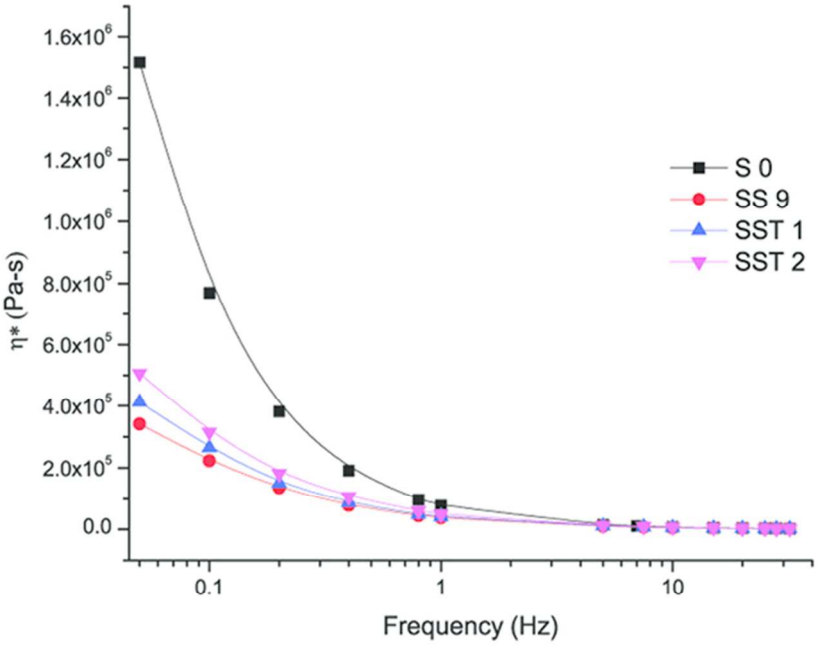

16
80x61mm (300 x 300 DPI)

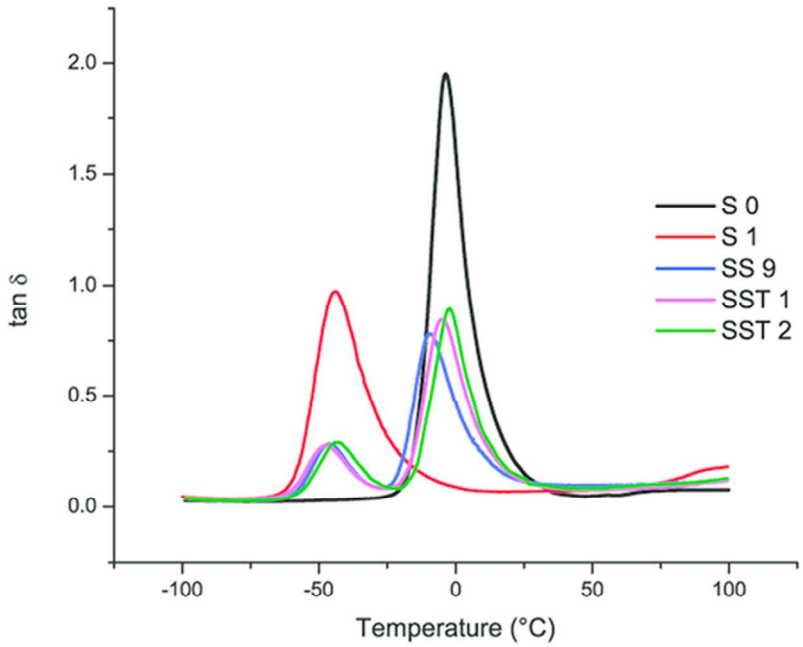

17
80x61mm (300 x 300 DPI)

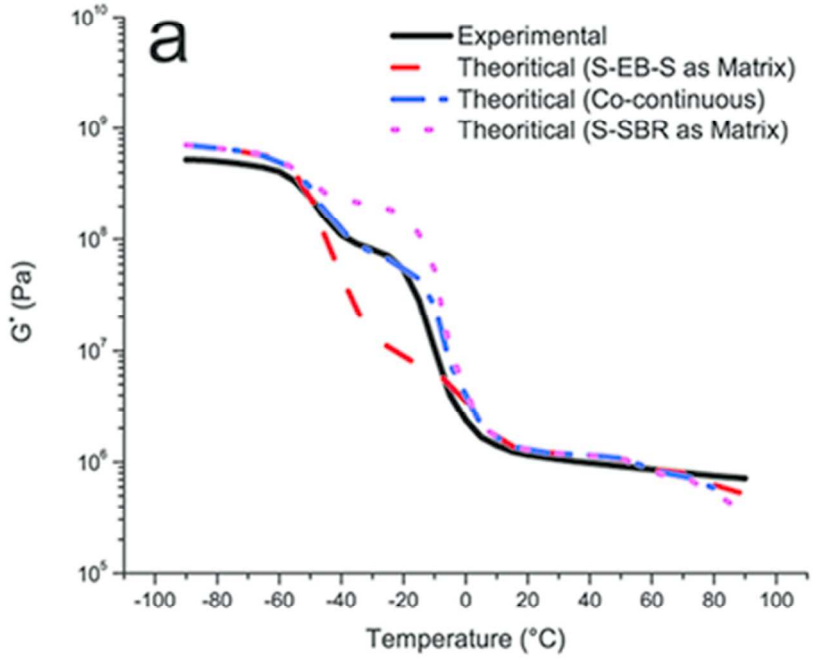

18(a)
79x61mm (300 x 300 DPI)

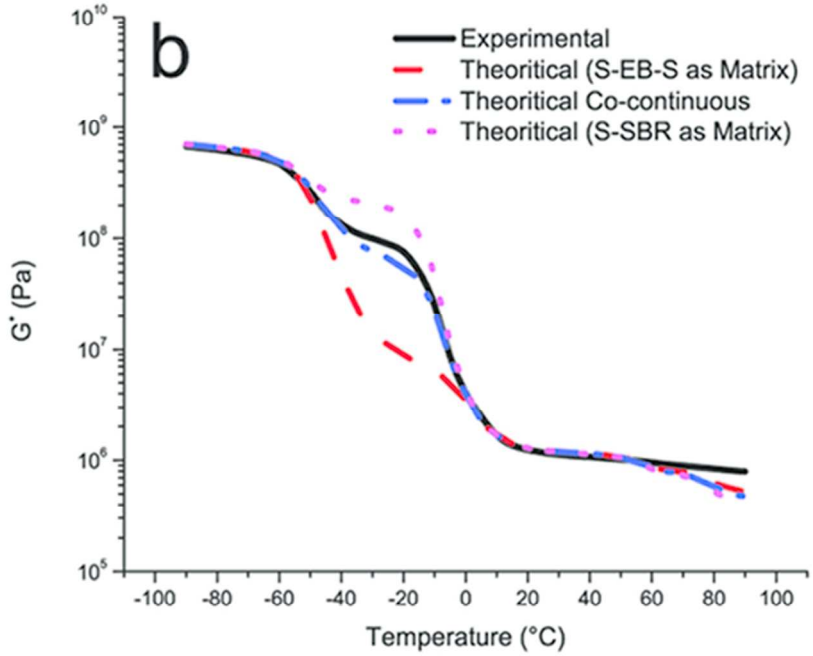

18(b)
80x61mm (300 x 300 DPI)

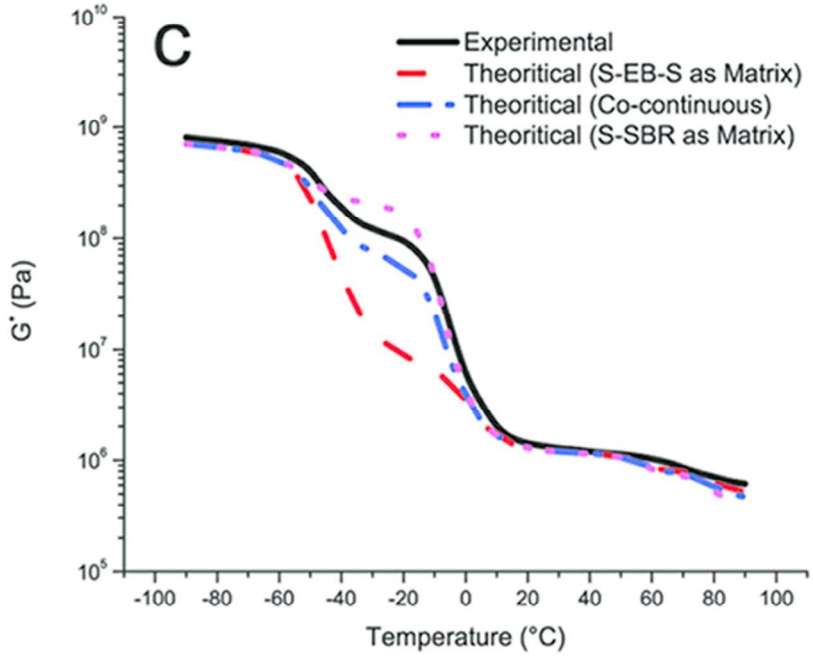

18(c)
80x61mm (300 x 300 DPI)

Table 1 - Factors and levels designed for S-EB-S and S-SBR (50:50) blends

Level \ Factor	A: Temperature (°C)	B: Rotor Speed (rpm)	C: Time (min)
1	160	60	10
2	180	80	8
3	200	100	6

Table 2 - Experimental layout based on Taguchi L_9 model

Blend Ratio	Experiment	Sample Number	Temperature (°C)	Rotor Speed (rpm)	Time (min.)
50:50	1	SS 1	1 160	1 60	1 10
	2	SS 2	1 160	2 80	2 8
	3	SS 3	1 160	3 100	3 6
	4	SS 4	2 180	1 60	2 8
	5	SS 5	2 180	2 80	3 6
	6	SS 6	2 180	3 100	1 10
	7	SS 7	3 200	1 60	3 6
	8	SS 8	3 200	2 80	1 10
	9	SS 9	3 200	3 100	2 8

Table 3: Compounding recipe of S-EB-S/ S-SBR TPVs (In phr*)

Ingredients	Function	Sample ID		
		S 0	SST 1	SST 2
S-SBR	Elastomer	100	100	100
S-EB-S	Thermoplastic Elastomer	-	100	100
ZnO	Accelerator activator	4	4	4
Stearic Acid	Accelerator activator	1	1	1
CBS	Accelerator	1	1	1
TMTD	Accelerator	0.5	-	0.5
Sulphur	Cross-linking agent	1	1	1

*phr: parts per hundred parts of elastomer.

Table 4 – Mechanical properties of EB 2, i.e. 50:50 S-EB-S/S-SBR blends as per Taguchi L_9 methodology

SEBS/SSBR (Wt %)	Sample ID	Tensile Strength (MPa)	EB (%)	100% Modulus (MPa)	200% Modulus (MPa)	300% Modulus (MPa)	Hardness (Shore A)
50/50	SS 1	4.4	1082	0.8	0.9	1.0	51
	SS 2	3.9	1039	0.8	0.9	1.0	51
	SS 3	3.5	835	0.8	0.9	0.9	51
	SS 4	3.6	1010	0.8	0.9	1.0	50
	SS 5	3.2	976	0.8	0.9	1.0	51
	SS 6	3.4	749	0.9	1.3	1.8	53
	SS 7	3.1	858	0.9	1.1	1.2	53
	SS 8	3.3	565	0.9	1.4	1.9	53
	SS 9	2.8	389	1.0	1.6	2.2	54

Table 5: Response Table for Signal to Noise Ratios - Higher is better (Tensile Strength)

Level	Temperature	Rotor Speed	Time
1	10.883	11.274	11.29
2	10.62	10.765	10.63
3	9.714	9.177	9.296
Delta	1.169	2.097	1.993
Rank	3	1	2

Table 6: Response Table for Signal to Noise Ratios - Higher is better (Elongation at Break)

Level	Temperature	Rotor Speed	Time
1	59.82	59.81	57.74
2	59.12	58.39	57.41
3	55.17	55.91	58.96
Delta	4.65	3.91	1.56
Rank	1	2	3

Table 7: Response Table for ANOVA analysis (Tensile Strength)

Source	DF	Seq SS	Adj SS	Adj MS	F-ratio	P-value	P_C (%)
Temperature	2	0.44	0.4356	0.2178	1.96	0.34	16.99
Rotor Speed	2	1.02	1.0156	0.5078	4.57	0.18	39.38
Time	2	0.91	0.9089	0.4545	4.09	0.20	35.14
Error	2	0.22	0.2222	0.1111			8.49
Total	8	2.59					

DF: degree of freedom, Seq SS: sequential sum of squares, Adj SS: adjusted (partial) sum of squares, Adj MS: adjusted (partial) mean squares, P_C: percentage contribution.

R-Sq = 91.39%

Table 8: Response Table for ANOVA analysis (Elongation at Break)

Source	DF	Seq SS	Adj SS	Adj MS	F-ratio	P-value	P_C (%)
Temperature	2	245501	245501	122750.5	22.86	0.042	56.72
Rotor Speed	2	162209	162209	81104.5	15.10	0.062	37.47
Time	2	14406	14406	7203.0	1.34	0.427	3.33
Error	2	10741	10741	5370.5			2.48
Total	8	432856					

DF: degree of freedom, Seq SS: sequential sum of squares, Adj SS: adjusted (partial) sum of squares, Adj MS: adjusted (partial) mean squares, P_C: percentage contribution.

R-Sq = 97.52%

Table 9 – Mechanical properties of sulphur cured TPVs (Standard deviation values for five numbers of test specimen are given in parenthesis)

Sample Name	Tensile Strength (MPa)	EB (%)	100% Modulus (MPa)	200% Modulus (MPa)	300% Modulus (MPa)	Hardness (Shore A)
S 0	1.8 (0.15)	338 (37.05)	0.7 (0.12)	1.1 (0.06)	1.5 (0.08)	48 (0.62)
SST 1	4.8 (0.62)	672 (79.79)	0.9 (0.03)	1.4 (0.03)	2.0 (0.05)	52 (0.84)
SST 2	4.9 (0.38)	533 (42.03)	1.1 (0.03)	1.7 (0.06)	2.6 (0.09)	55 (0.71)

Table 10: Dynamic mechanical properties of TPVs, rubber vulcanizate and pristine TPE

Sample Name	Storage Modulus (E′) (MPa)			Tanδ		
	−50°C	0°C	+50°C	−50°C	0°C	+50°C
S 0	1849.31	12.19	2.31	0.03	1.70	0.05
S 1	267.37	5.04	4.02	0.72	0.09	0.08
SS 9	610.87	6.23	2.69	0.26	0.47	0.10
SST 1	713.70	9.29	3.00	0.24	0.71	0.08
SST 2	1103.21	13.13	3.33	0.18	0.82	0.08

Table of contents

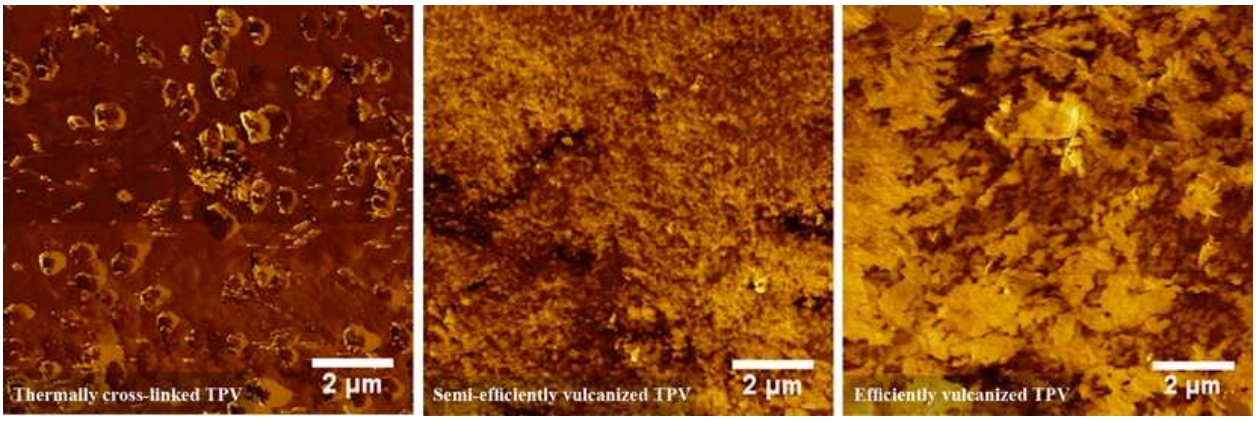

Novel thermally cross-linked and sulphur vulcanized TPVs based on S-EB-S and S-SBR blends have registered good mechanical and dynamic mechanical properties with reduced hardness suitable for automotive applications.

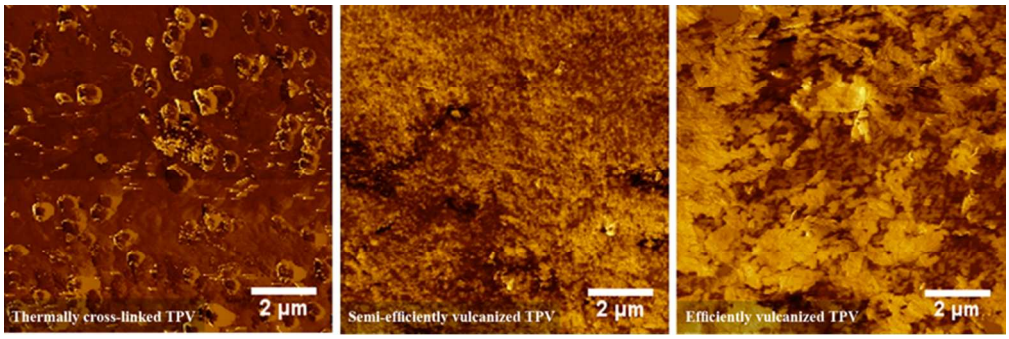

70x23mm (300 x 300 DPI)